Immunological landscape of human lymph nodes during *ex vivo* measles virus infection

Joshua A Acklin[1,2], Aum R Patel[1,2], Shu Horiuchi[1], Arianna S Moss[1], Andrew P Kurland[1], Patricia Thibault[1], Emma J Degrace[1,2], Satoshi Ikegame[1], Jillian Carmichael[1], Naoko Imai[1], Hideki Ueno[1], Benjamin Tweel[3], Jeffrey R Johnson[1], Brad R Rosenberg[1], Benhur Lee[1], and Jean K Lim[1]

AFFILIATIONS:

[1] Department of Microbiology, Icahn School of Medicine at Mount Sinai, New York, NY, United States

[2] Graduate School of Biomedical Sciences, Icahn School of Medicine at Mount Sinai, New York, NY, United States

[3] Department of Otolaryngology, Icahn School of Medicine at Mount Sinai, New York, NY, United States

ABSTRACT:

Lymph nodes are the primary site of replication for measles virus (MeV). Here, we modeled MeV infection in human tonsil explants, utilizing a clinical strain of MeV that expresses GFP. We show that MeV replicates efficiently in this tissue as measured by increasing infectious virus production and GFP^+ cells (>10% of tonsillar cells by day 8). Using scRNA-Seq, we identified 29 cell populations, all of which were susceptible to MeV. While T cells were the most abundant cell type in the lymphoid explants, B cells were the dominant infected population. Flow cytometry analysis revealed that the preferential infection of B cells was associated with higher CD150 expression. We found that while germinal center B cells were the largest population of infected B cells, there were no differences in susceptibility to MeV among individual B cell subsets. Among $CD3^+$ T cells, infection in both the $CD4^+$ and $CD8^+$ compartments displayed bias towards antigen experienced subsets and away from naive cells, consistent with relative CD150 expression. Differential gene expression analysis revealed that the host response to MeV was dominated by the potent induction of interferon stimulated genes within both T and B cells. These data provide new insights into how MeV infection progresses in lymph nodes, a critical launching point for pathogenesis.

Author Summary

Measles virus (MeV) is a re-emerging pathogen that has dramatic disease outcomes in children. Immunological amnesia is a dangerous disease outcome that is caused by MeV infection of lymphocytes. Here, we infect human tonsil explants with a GFP-expressing clinical isolate of MeV to assess the immunological events that occur during infection of this critical site. Using single-cell RNA sequencing, we identified 29 distinct populations of tonsillar cells that are susceptible to MeV infection. Further immunophenotyping revealed a preferential infection of B cell lineages compared to T cell lineages, and that among T cells, memory cells are preferential targets of infection compared to naïve counterparts. Taken together, our data thoroughly characterize the infectious and immunological events that shape disease progression in lymph nodes and identify cellular susceptibilities to MeV infection which may be critical in the development of antivirals for MeV.

CONFLICTS OF INTEREST

The authors have declared that no conflict of interest exists.

50 **INTRODUCTION:**

51 Measles virus (MeV) is the most infectious virus known to infect humans, with a reported R_0 value
52 of 12-18(1-7). MeV outbreaks have largely been controlled with the advent of the two-dose
53 measles, mumps, and rubella (MMR) vaccine, yet MeV still causes ~200,000 deaths annually,
54 primarily among unvaccinated children in developing countries(8-10). However, recent surges in
55 vaccine-hesitancy have allowed for MeV to re-emerge in countries like the United States and the
56 United Kingdom, where the MMR vaccine coverage has historically been high(11-14). Global
57 vaccination campaigns for MeV have been stalled due to the COVID-19 pandemic, increasing the
58 risk of MeV outbreaks globally (15). There are currently no licensed directed antivirals for MeV(16,
59 17).

60 MeV is a morbillivirus of the family *Paramyxoviridae* that is transmitted through the
61 respiratory tract, where alveolar macrophages and dendritic cells are the initial cellular targets of
62 infection(18, 19). These infected immune cells then traffic to the draining lymph nodes where the
63 virus replicates rapidly in lymphocytes that express the entry factor CD150/SLAMF1(20-24). MeV
64 is also known for causing immune amnesia through the depletion of $CD150^+$ B and T cells in both
65 primary and secondary lymphoid organs, increasing the morbidity and mortality rates from
66 secondary infections with unrelated childhood pathogens(25-32). Immunological amnesia
67 following MeV infection has been shown to significantly reduce the antibody repertoire towards
68 common childhood pathogens, rendering these children essentially naïve against viruses such as
69 the human parainfluenza viruses, respiratory syncytial virus, coronaviruses, and
70 cytomegalovirus(33). Given that immune responses are primarily generated in the draining lymph
71 node, and that this site is a critical launching pad for MeV infections, understanding virus:host
72 interactions at this site is paramount for the identification of factors that shape disease
73 progression.

74 Early work on the tropism of MeV in lymphoid cells focused on the role of T cells, as the
75 original reports of immunological amnesia were based on the lack of memory T cell

responsiveness to cognate antigen following a MeV infection(34, 35). *In vitro* characterization of MeV infection in primary lymphocytes revealed that B cells are the most extensively infected population of lymphocytes, while $CD4^+$ and $CD8^+$ T cells are less likely to become infected, consistent with their relative CD150 expression(36). Characterization of MeV infection in PBMCs from both humans and macaques further demonstrated the proclivity of MeV for lymphocytes and clearly demonstrated that MeV infection is biased towards memory lymphocytes as compared to their naïve counterparts, which was subsequently validated in PBMCs derived from MeV-infected children(18, 31, 37, 38).

While these studies provide insights into the susceptibility of circulating lymphocytes to MeV, these works are limited in that they do not examine infection within the 3-dimensional architecture of secondary lymphoid tissue. The draining lymph node is a complex structure containing high density B cell follicles surrounded by T cell zones(39).The density and distribution of $CD150^+$ cells within the structure of the lymph node may be important in determining *in vivo* cellular susceptibility as well as the kinetics of lymph node infection. Studies in macaques have examined the geographic distribution of infected cells within secondary lymphoid tissues and have identified that the majority of infection is established within B cell follicles(38). Further, these studies recapitulated the heightened susceptibility to infection among memory, but not naïve lymphocyte subsets within secondary lymphoid organs(38). To approach this question in human lymph nodes, studies using human tonsil explants have been conducted, where lymphoid tissue structures and native cell ratios are intact. These studies similarly found that B cells are a preferential target of MeV infection(40, 41). Additionally, these works also concluded that memory T cells were more extensively infected compared to naive T cell subsets; however no further phenotyping of these cells was conducted(40). To fill these gaps, we revisit the tonsil model with a GFP expressing clinical isolate of MeV to immunophenotype infected cells over time, with greater granularity than ever before. While single cell RNA sequencing (scRNA-seq) of MeV infected airway epithelium has been conducted(42), we here define the immunological landscape

102 of MeV infected human lymph nodes with single cell resolution for the first time. Our findings both
103 deepen our understanding of the different cell types that are susceptible to MeV, as well as reveal
104 transcriptional signatures of MeV infected cells with single cell resolution in human lymph nodes.

105 **RESULTS**

106 **MeV robustly infects human lymphoid tissues *ex vivo*:**

107 Given that tonsils serve as a draining lymph node, we sought to utilize these tissues to examine
108 MeV infection within the native architecture of human lymph nodes. Tissue samples from routine,
109 non-inflamed tonsillectomies were cut into 2mm cubes and then placed on collagen beds as
110 previously described(43). After 24hrs, individual tissue blocks were infected with a clinical isolate
111 of MeV, IC323, which was engineered to express GFP at the 3' end of the viral genome(44). To
112 assess the extent to which MeV could replicate in human lymphoid tissues across multiple donors
113 (n=11), we collected culture supernatants at days 3, 6 and 8 post infection and measured
114 infectious virus production by fluorescent plaque assay. As shown in Fig 1A, viral titers increased
115 for all donors, with ~ 2.5 log increase over the 8-day culture.

116 To assess the extent of infection within the tissues, and to further confirm productive
117 infection, we measured the frequency of GFP^+ cells over time by flow cytometry. As shown in **Fig**
118 **1B**, the percentage of GFP^+ cells increased over time, while no GFP^+ cells were detected in the
119 uninfected condition. The percentage of GFP^+ cells was quantified across a total of 3 donors,
120 revealing a high frequency of MeV-infected cells by day 8 post infection (**Fig 1C**). We also
121 histologically evaluated infection utilizing *in situ* hybridization to examine the presence of GFP
122 RNA. As shown with one representative donor, RNA transcripts for GFP were readily detected
123 within the tissue samples (**Fig 1D**). Together our data establish that human tonsils infected *ex*
124 *vivo* are highly susceptible to MeV in the absence of any stimulation or infection enhancers,
125 providing us with a robust model system to further characterize MeV-infected cells.

126 **ScRNA-Seq of MeV-infected tissues reveals broad cellular susceptibility:**

127 Given that MeV productively infected the human tonsil explants, we next sought to directly
128 compare MeV-infected cells to uninfected cells using scRNA-Seq. Briefly, we generated single
129 cell suspensions from infected and donor-matched uninfected conditions on day 8 post infection,
130 the time point at which the maximum number of infected cells was observed. We sorted GFP^+
131 (infected) and GFP^- (bystander) cells from the MeV-infected condition, as well as the GFP^- cells
132 (uninfected) from the uninfected condition for scRNA-Seq using a workflow shown in **Fig 2A**. We
133 validated the quality of sequencing across the three groups by quantifying unique molecular
134 identifier (UMI) counts, unique genes captured, and the representation of mitochondrial transcripts
135 (**Fig S1 A-C)**. As expected, only cells from the infected group had detectable MeV transcripts (**Fig**
136 **2B**). Among the infected cells, we examined the expression levels of viral transcripts as a final
137 confirmation of infection status. Infected cells showed a transcriptional gradient of viral genes
138 from 3' to 5', consistent with the phenomenon of run-off transcription that occurs for
139 paramyxoviruses (**Fig 2C**). To our knowledge, this is the first time that MeV transcriptional
140 gradients have been reported at single cell resolution.

141 Following data integration, we annotated constituent cell types across conditions based
142 on immune cell reference data and supervised differential marker gene analysis (see *Methods*).
143 Using this strategy, we identified 29 distinct populations of cells (**Fig 2D**), with the vast majority
144 belonging to either T cell or B cell subsets (annotation strategy shown in **Fig S1D**). Surprisingly,
145 GFP^+ cells were found in all 29 populations. Indeed, we were able to subsets of regulatory T cells
146 and B cell subpopulations susceptible to infection and capturing cell types not previously
147 described as targets of MeV infection (**Fig 2E**). Quantification of the frequency of each of these
148 populations within uninfected, bystander and infected cell sorted sample groups revealed that,
149 despite T cells comprising the largest population of cells in human tonsils (as shown in uninfected
150 and bystander groups), they were a minority among the MeV-infected cells. Instead, IgD^+ B cells
151 were overrepresented within the pool of GFP^+ cells (**Fig 2F**). In fact, we observed a reduction in

152 the frequency of all T cell subsets among all infected cells. These data suggest that either T cells
153 have a broadly lower susceptibility to MeV infection compared to B cells, or that MeV kills T cell
154 targets prior to day 8. Finally, we quantified the percentage of UMI counts that mapped to MeV
155 UMIs for each identified cell population to assess the extent to which the transcriptome is coopted
156 for viral gene expression. As shown in **Fig 2G**, MeV transcripts constituted ~2% of all transcripts
157 for each cluster on average. These data collectively reveal that MeV has a wide cellular tropism
158 within the architecture of the lymph node and suggest that B cells may have heightened
159 susceptibility to infection, relative to other cells present.
160
161 **B cells are preferential targets of MeV infection in lymph nodes infected *ex vivo*:**
162 The data from the scRNA-Seq analysis suggested that differences in susceptibility to MeV may
163 exist within the *ex vivo* infected tonsil tissues. However, these data were limited in that they only
164 assessed late-stage (day 8) infected cells. Therefore, to examine the possible changes that may
165 occur over time, as well as susceptibility to infection, we designed immunophenotyping panels to
166 phenotype cell subsets identified in the scRNA-Seq dataset using flow cytometry (n=3 donors).
167 Other groups have assessed the percentage of MeV-infected cells among individual cell
168 subsets(18, 31, 36, 38, 40, 41, 45). While this approach has revealed general differences in
169 susceptibility, it does not account for the relative contribution of each population to the total
170 infection pool. Here, we evaluated MeV infection in tonsils in two ways: 1) we quantified the
171 absolute frequency of each identified cell subset within both the uninfected and GFP+ (infected)
172 populations found within the tonsils (**Table 1**). This analysis allows us to see the contribution of
173 each cell subset to the total infection pool. 2) We also quantified the relative frequency of each
174 identified cell subset within both the uninfected and GFP+ (infected) populations within the T and
175 B cell subsets (**Figs 3-7**). This analysis allows us to distinguish between general lineage
176 susceptibility and cell-type specific susceptibility.
177

178 **Table 1: Frequency of immune cell subsets among uninfected and MeV-infected cells**

	Day 3				Day 6				Day 8			
% Of CD45+ Cells	**Uninfected**		**GFP+**		**Uninfected**		**GFP+**		**Uninfected**		**GFP+**	
	Mean	**STDEV**	**Mean**	**STDEV**	**Mean**	**STDEV**	**Mean**	**STDEV**	**Mean**	**STDEV**	**Mean**	**STDEV**
CD19	*35.9*	*5.7*	*58.4*	*5.6*	*32.2*	*9.8*	*69.2*	*9.8*	*38.7*	*6.7*	*67.0*	*7.3*
GCBs	*16.9*	*6.7*	*24.5*	*5.2*	*14.8*	*7.8*	*31.9*	*12.3*	*18.7*	*9.4*	*36.1*	*13.1*
MBCs	*10.8*	*2.0*	*18.0*	*5.0*	*8.9*	*3.0*	*22.2*	*4.5*	*9.4*	*3.5*	*16.0*	*6.2*
AMBCs	*6.1*	*2.5*	*10.9*	*6.8*	*5.5*	*0.9*	*9.0*	*4.5*	*6.7*	*3.1*	*7.5*	*3.5*
Naïve	*2.1*	*0.3*	*5.0*	*2.6*	*3.0*	*0.9*	*6.2*	*0.6*	*3.9*	*1.3*	*7.3*	*3.2*
CD3	*59.9*	*8.0*	*20.2*	*9.5*	*64.9*	*10.0*	*23.7*	*10.4*	*58.0*	*7.3*	*26.8*	*5.8*
CD4	*41.6*	*12.0*	*13.4*	*6.9*	*52.8*	*9.9*	*14.6*	*3.6*	*46.9*	*6.8*	*13.1*	*3.0*
CXCR5+	*17.2*	*5.9*	*7.5*	*0.5*	*21.9*	*11.4*	*7.1*	*1.8*	*17.0*	*7.0*	*4.6*	*1.3*
CXCR5-	*23.8*	*6.3*	*5.8*	*6.6*	*30.3*	*2.8*	*7.5*	*2.7*	*29.7*	*8.2*	*7.5*	*4.3*
Naïve	*5.4*	*1.3*	*0.1*	*0.1*	*6.1*	*2.2*	*0.5*	*0.4*	*5.2*	*2.1*	*0.3*	*0.2*
T_{CM}	*5.2*	*3.3*	*1.5*	*2.4*	*5.8*	*3.3*	*1.2*	*0.7*	*6.2*	*3.0*	*0.9*	*0.5*
T_{EMRA}	*1.0*	*0.3*	*0.1*	*0.1*	*1.5*	*1.0*	*0.3*	*0.4*	*1.1*	*0.1*	*0.1*	*0.1*
T_{EM}	*11.9*	*2.6*	*3.6*	*3.3*	*17.2*	*3.8*	*5.5*	*1.6*	*17.0*	*8.4*	*6.1*	*4.1*
T_H1	*8.5*	*0.8*	*2.4*	*2.5*	*8.9*	*5.0*	*2.9*	*1.4*	*7.2*	*2.1*	*2.8*	*0.8*
T_H1*	*2.0*	*1.0*	*0.7*	*0.3*	*2.7*	*1.5*	*0.6*	*0.3*	*2.8*	*1.9*	*0.6*	*0.5*
T_H2	*0.8*	*0.4*	*0.4*	*0.4*	*3.4*	*1.7*	*1.4*	*1.0*	*3.9*	*3.1*	*2.1*	*1.9*
T_H17	*0.4*	*0.4*	*0.1*	*0.1*	*2.0*	*1.2*	*0.6*	*0.6*	*2.8*	*2.8*	*0.6*	*0.7*
CD8	*9.7*	*1.8*	*1.0*	*0.7*	*9.5*	*1.6*	*2.1*	*0.4*	*7.7*	*1.0*	*2.2*	*0.3*
Naïve	*3.2*	*1.1*	*0.1*	*0.1*	*3.1*	*1.1*	*0.2*	*0.1*	*2.6*	*1.2*	*0.2*	*0.2*
T_{CM}	*1.3*	*0.5*	*0.4*	*0.3*	*0.9*	*0.6*	*0.3*	*0.2*	*0.7*	*0.6*	*0.2*	*0.1*
T_{EMRA}	*4.1*	*0.7*	*0.5*	*0.3*	*4.5*	*0.8*	*1.5*	*0.1*	*3.7*	*0.7*	*1.4*	*0.5*
T_{EM}	*1.0*	*0.4*	*0.0*	*0.0*	*0.9*	*0.5*	*0.2*	*0.1*	*0.7*	*0.4*	*0.1*	*0.1*
DN	*7.4*	*3.1*	*1.7*	*2.2*	*2.2*	*1.4*	*0.7*	*0.5*	*2.9*	*1.6*	*1.2*	*0.7*
DP	*0.3*	*0.1*	*3.4*	*0.9*	*0.4*	*0.3*	*4.4*	*5.0*	*0.4*	*0.2*	*5.2*	*3.1*
CD19-/CD3-	*2.9*	*2.0*	*1.9*	*0.6*	*2.2*	*0.5*	*2.3*	*0.4*	*2.9*	*0.6*	*3.0*	*0.0*

179

180 The first broad stratification was to quantify the frequency of B cells and T cells (gating
181 schemata shown in **Fig 3A**). As shown in **Fig 3B** and **Table 1**, there was a significantly higher
182 frequency of $CD19^+$ cells among the GFP^+ cells (~58% at day 3) compared to their frequency in
183 the total uninfected population (~36% at day 3; $p<0.0001$). This difference was established early
184 in infection and maintained at all three time points. Conversely, we observed a decrease in the
185 frequency of $CD3^+$ cells (**Fig 3C** and **Table 1;** ~60% among uninfected cells and ~20% among
186 GFP^+ cells; $p<0.0001$).

187 We wondered whether this increase in B cell susceptibility was associated with the
188 expression of CD150, the lymphocyte entry factor for MeV. To measure this, we assessed the
189 mean fluorescence intensity (MFI) of CD150 on the $CD19^+$ B cells and $CD3^+$ T cells from the
190 uninfected condition at day 6, to control for any alteration in CD150 expression that may occur
191 upon MeV infection as well as any change that may occur as a result of *ex vivo* culture conditions
192 as previously shown(46, 47). We found that $CD19^+$ B cells express significantly higher levels of
193 CD150 compared to $CD3^+$ T cells (**Fig 3D**). Consistent with previous reports, these data suggest
194 that the increased susceptibility to MeV infection among B cells may be due to the expression of
195 CD150(36, 38, 40). These data extend our findings in **Fig 2**, as they reveal that susceptibility to
196 infection is positively associated with CD150 expression, reducing the likelihood that the
197 difference in T cell frequency between the uninfected condition and GFP+ cells is due solely to
198 cell killing.
199
200 **B cell subsets found within lymph nodes are not differentially susceptible to MeV:**
201 Given that lymphoid tissues are composed of various B cell subpopulations, we next asked
202 whether MeV susceptibility differed among these B cell subsets. To test this, we further
203 immunophenotyped $CD19^+$ B cells based on the expression of CD38 and CD27 (gating schemata
204 shown in **Fig 4A**), which allows for the differentiation of germinal center B cells (GCBs;
205 $CD38^+CD27^-$), activated memory B cells (AMBCs, $CD38^+CD27^+$), memory B cells (MBCs; $CD38^-$
206 $CD27^+$)) and naive B cells ($CD38^-CD27^-$). Quantification of the frequency of these subpopulations
207 among all $CD19^+$ cells in both the uninfected tonsil and GFP^+ condition revealed no skewing of
208 MeV-infection within any B cell subsets, except for MBCs at the day 8 time point (**Fig 4B-E**),
209 where MBCs were found less frequently among GFP^+ B cells than among uninfected B cells.
210 Quantification of CD150 expression across these B cell subsets showed that only MBCs had a
211 significantly lower expression, which may account for the lower frequency of MeV-infection in this
212 population at day 8 (**Fig 4F**).

213 The scRNA-Seq analysis, as shown in **Fig 2G,** identified IgD$^+$ B cells as the largest
214 population of MeV-infected cells, but we were unable to further subset this cluster. Guided by this
215 knowledge, we next asked how each identified B cell population contributed to the total infection
216 pool. We found that the largest population of infected B cells in the explants are GCBs, comprising
217 ~24.5% of the GFP$^+$ cells on day 3, and increasing to 36.1% by day 8 (**Table 1**). The majority of
218 these cells were IgD$^+$, consistent with our scRNA-Seq findings (data not shown).
219
220 **T cell subsets show differential susceptibility to MeV:**
221 While T cells are the predominant cell type found in the human tonsil explants, we found that the
222 frequency of T cells among the GFP$^+$ cells was significantly reduced compared to the frequency
223 among uninfected cells (**Fig 3C** and **Table 1**). To determine whether this effect was driven by
224 specific T cell subsets, or if it was a generalized lower frequency among the T cell lineage, we
225 first evaluated the CD4$^+$ and CD8$^+$ T cells compartments (gating schemata shown in **Fig 5A**). We
226 found that while CD4$^+$ T cells were the largest population of T cell in the explants (~41.6% of all
227 events at day 3; **Table 1**), the proportion of CD4$^+$ T cells among the CD3$^+$ population was
228 unchanged between the uninfected and infected conditions (**Fig 5B**), apart from a potent
229 decrease in frequency at day 8. Analysis of CD8$^+$ cells revealed a similar reduction in frequency
230 among infected T cells compared to uninfected T cells, which was significant at day 3 post
231 infection (**Fig 5C**). While no differences in susceptibility were noted among the CD4$^-$CD8$^-$ double
232 negative (DN) T cells (**Fig 5D**), we did identify a significantly higher frequency of CD4$^+$CD8$^+$
233 double positive (DP) T cells at day 3 post infection, consistent with previous reports from thymus
234 (**Fig 5E**)(45). Though rarely reported on, these DP T cells have been shown to arise in both
235 PBMCs and lymph nodes from CD8 re-activation among CD4$^+$ T cells, in both pathogenic and
236 non-pathogenic states(48). While the function of these cells is not well understood, our data
237 suggest that they are prevalent within the MeV infected condition, perhaps resulting from viral
238 modulation of CD4/CD8 expression. In addition to being more frequent in the total tonsil explant,

239 $CD4^+$ T cells were found to express more CD150 than $CD8^+$ T cells (**Fig 5F**). DN T cells expressed
240 similar levels of CD150 to $CD4^+$ cells, however DP T cells trended towards highest expression,
241 perhaps accounting for heightened susceptibility at day 3.

242 Next, we sought to examine if there were any differences in susceptibility to infection
243 among the $CD4^+$ T cells (gating schemata shown in **Fig 6A**). Consistent with previous reports on
244 the cellularity of human tonsils isolated from young adults, $CXCR5^+$ T cells (consisting of both
245 pre-T_{FH} and T_{FH} cells) are the most frequent subset of $CD4^+$ cells in our explants (**Table 1**)(49).
246 After accounting for their representation among $CD4^+$ T cells, we found no differences in
247 susceptibility to infection based on CXCR5 status (**Fig S2A-B**), despite $CXCR5^+$ cells expressing
248 significantly more CD150 than $CXCR5^-$ cells (**Fig S2C**). Gating next on the $CXCR5^-$ cells, we
249 tested if there were any differences in susceptibility among $CXCR5^-$ T cell subsets. We identified
250 naive $CD4^+$ cells at a significantly lower frequency among infected $CXCR5^-$ cells than among
251 uninfected at all time points (**Fig 6B**). In contrast, T_{EM} cells trended towards a higher frequency
252 among infected $CXCR5^-$ cells than among uninfected at all time points, although this trend did not
253 reach statistical significance (**Fig 6C**). T_{CM} and T_{EMRA} cells were found to be infected at the rate
254 they were present among uninfected $CXCR5^-$ T cells (**Fig 6D-E**). CD150 expression was
255 significantly higher in T_{EM} cells than among naive $CD4^+$ cells (**Fig 6F**), and while expression on
256 T_{CM} and T_{EMRA} cells trended towards higher expression than naïve $CD4^+$ cells, this trend did not
257 reach statistical significance. Further phenotyping of these T_{EM} cells into T_h cell subsets revealed
258 no differences in susceptibility (gating schemata shown in **Fig S3A**, susceptibility in **Fig S3B-E**),
259 despite varying degrees of CD150 expression (**Fig S3F**). Taken together, these data show that
260 naive $CD4^+$ cells are less susceptible to MeV infection relative to their mature counterparts, with
261 no differences in susceptibility among T_{EM} subsets.

262 Finally, to determine susceptibility among $CD8^+$ T cells, we further immunophenotyped
263 $CD8^+$ cells based on CD45RA and CCR7 expression into: T central memory (T_{CM}; $CD45RA^-$
264 $CCR7^+$), T Effector memory (T_{EM}; $CD45RA^-CCR7^-$), T effector memory RA^+ (T_{EMRA};

265 CD45RA$^+$CCR7$^-$) and naive CD8$^+$ cells (CD45RA$^+$CCR7$^+$; gating strategy shown in **Fig 7A**).
266 Similar to what was observed among CD4$^+$ cells, naive CD8$^+$ cells were found less frequently
267 among infected CD8$^+$ cells than among uninfected at all time points (**Fig 7B**). Reciprocally, there
268 was a higher frequency of CD8$^+$ T_{EM} cells at days 6 and 8 post infection, indicating preferential
269 infection (**Fig 7C**). CD8$^+$ T_{EM} and T_{EMRA} cells showed no differences in susceptibility (**Fig 7D-E**).
270 Quantification of CD150 expression revealed no significant differences in expression among the
271 CD8 subsets, although TCM cells trended towards higher expression (**Fig 7F**).
272
273 **MeV induces a canonical interferon driven response in both B and T cells:**
274 While we identified several cell types that demonstrated altered susceptibility to MeV infection,
275 the most striking differences were between B and T cells (**Figs 2 and 3**). We were able to assess
276 the expression of CD150 via flow cytometry as one explanation of differential susceptibility to
277 infection, however we also wondered whether there were any differences in the host response to
278 infection among these cell types that may account for differences in susceptibility. To ask this, we
279 probed the scRNA-Seq data, where we randomly sampled an equal number of B cells or T cells
280 from the uninfected, bystander and infected groups, and conducted differential gene expression
281 analysis. As a proof of principle, the most significantly induced genes among the infected cells
282 were MeV genes and GFP transcripts (**Fig 8A-B**). Excluding viral genes, the most significantly
283 upregulated transcripts among GFP$^+$ cells were associated with a canonical IFN signature.
284 Interestingly, this pattern of interferon induction was also observed among bystander cells, which
285 were isolated from the infected tissue condition but do not contain viral transcripts. This was true
286 for both B and T cells. We detected MeV interferon antagonist transcripts, V and C, but were
287 unable to make meaningful comparisons in the expression of these transcripts among infected
288 cell types due to the low read coverage at the p-editing site (**Fig S4**). To validate this interferon
289 response, we conducted qRT-PCR comparing the RNA isolated from the infected and uninfected
290 tissues of two additional tonsil donors over time. We evaluated the expression of IFIT1, IFIT3 and

291 MX1, three of the highly expressed type-I interferon stimulated genes (ISGs) from the scRNA-
292 Seq analysis. As shown in **Fig 8C-E**, we found potent induction of all three genes by day 8 post
293 infection, the time point of scRNA-Seq. These findings are contrary to previously reported
294 microarray findings in PBMCs isolated from infected people, where no interferon response was
295 observed(50-55). Taken together, our data suggest that MeV induces a potent interferon
296 response at the transcriptional level in both infected and bystander B and T cells, with no notable
297 differences that account for the increased susceptibility of B cells.

298 **DISCUSSION**

299 Measles virus pathogenesis is dependent upon early replication within the draining lymph node,
300 yet our understanding of how infection proceeds in this organ and its link to immunologic amnesia
301 is incomplete(50). In this study, we sought to model MeV infection within the 3-dimensional
302 architecture of human lymph nodes, comprehensively identifying the immunological events that
303 occur during MeV infection. *Ex vivo* infection of human tonsil explants with a GFP-expressing
304 clinical strain of MeV resulted in a high frequency of GFP^+ cells, thus allowing for sorting of
305 infected cells and downstream scRNA-Seq analysis. To our knowledge, this is the first report of
306 scRNA-Seq on MeV infected lymphocytes. This unbiased approach revealed that all cell types
307 identified within the lymph nodes were susceptible to MeV infection, albeit to different degrees.
308 Despite being a minority of cells within the tonsil explants, B cells were the most frequently
309 infected cell type, suggesting a heightened susceptibility to infection compared to other cell types
310 present. In contrast, T cells were less likely to become infected with MeV. Using flow cytometry,
311 we confirmed these findings across multiple donors and extended these results to show that this
312 difference in susceptibility to infection was established early in infection and remained constant
313 over time. Ultimately, our findings in this model advance and deepen our understanding of how
314 infection progresses within this critical site of viral replication.

315 Previous studies on MeV pathogenesis have largely focused on the infection of T cells
316 within secondary lymphoid tissue(31, 36, 37, 40, 45, 56). Indeed, immunological amnesia was
317 originally described as a T cell phenotype, whereby children that had previously tested positive
318 for a hypersensitivity test to tuberculin antigen began to test negative following measles
319 infection(34). Subsequent work in thymus and macaques revealed that MeV preferentially infects
320 and depletes memory T cells over naive T cell subsets(38, 45). While we do recapitulate that
321 antigen experienced/memory subsets of T cells were more frequently infected with MeV than
322 naïve subsets, we also identified that the vast majority of infection in secondary lymphoid tissue
323 is within B cells. We therefore postulate that these cells may be the most important targets for
324 infection at this site. Consistent with this notion, recent reports demonstrate that MeV-infected
325 children lose a large proportion of their antibody repertoire to common childhood pathogens
326 following MeV infection(33). We found that memory B cells were large targets of infection in these
327 explants, supporting the idea that MeV infection can impact the antibody repertoire(36, 57).
328 However, we also found that germinal center B cells (GCBs) were by far the largest population of
329 infected cells in the lymph node explants. These are the cells that are capable of mounting new
330 germinal center responses upon interaction with T follicular helper cells (T_{FH})(39). Therefore,
331 these findings raise the possibility that future germinal center responses may also be impacted
332 by the infection and/or depletion of this compartment.

333 To this point, we also uncovered that $CD4^{+}CXCR5^{+}$ (Pre-T_{FH} and T_{FH}) cells were major
334 targets of infection, being the largest infected T cell subset in the explants. Previous reports
335 utilizing dissociated tonsils found that these cells were not major targets of infection relative to
336 other T cell subsets(36), consistent with our finding that CD4+ cells do not have altered
337 susceptibility to MeV based on CXCR5 status. It remains, however, that while these are not
338 preferential infection targets, our data demonstrate that they are the largest targets among T cells.
339 As CXCR5 is involved in T cell trafficking into germinal centers, we wonder if this discrepancy is
340 a result of the fact that our system maintains the architecture of the lymph node. One hypothesis

341 is that the proximity of CXCR5$^+$ cells to infected GCBs could be responsible for the extent of
342 infection within the CXCR5$^+$ cells. If this were true, it would raise new questions about the role of
343 these cells in MeV pathogenesis, as infection and/or depletion of CXCR5$^+$ T helper cells could
344 diminish the ability to form *de novo* germinal center responses.

345 Many groups have implicated CD150 expression as the primary driver of lymphocyte
346 susceptibility to MeV infection(18, 20, 21, 36, 37, 45, 50, 56). Our data are generally consistent
347 with this notion, as we found that B cells generally express higher levels of CD150 than T cells,
348 and that among infected T cell subsets, susceptibility to infection trends with CD150 expression.
349 However, we also identified that among B cell subsets, CD150 expression was not associated
350 with susceptibility. This finding suggests that there may be a threshold of CD150 expression
351 beyond which higher expression does not induce higher susceptibility. Given the distinct
352 localization patterns of B cell subsets within lymphoid tissue, we postulate that this threshold could
353 be a result of the geographical distribution and/or density of CD150 expressing cells within the
354 lymph node. Future work should be conducted utilizing spatial transcriptomic or proteomic
355 technologies to assess the impact of the architectural context of MeV infection in determining how
356 disease progresses.

357 A confounding factor in evaluating cellular susceptibility to infection is distinguishing
358 whether observed differences are a result of factors specific to that cell type, or a broader lineage
359 susceptibility. An excellent example of this would be among the T cells, which we found to be
360 generally less frequent among the MeV-infected cells than the uninfected cells. Because of this,
361 CXCR5$^+$ T cells are found significantly less frequently among the MeV-infected cells than
362 uninfected cells. However, by first subsetting on CD4$^+$ T cells, we were able to see that this was
363 not specific to CXCR5$^+$ T cells, and instead was driven by a generalized low infection rate among
364 all T cell subsets. On the other hand, this approach also revealed interesting subpopulations of
365 cells which have heightened susceptibility to infection, such as CD8$^+$ T_{EM} cells. Ultimately, these

366 data revealed different cell subsets that may be of interest for the development of targeted antiviral
367 therapies.

368 As a successful human pathogen, MeV must either evade the induction of a host
369 response, shut down the induced response, or utilize that response for its own benefit. Previous
370 groups have shown that MeV does not induce a potent interferon (IFN) response, as the viral V
371 and C proteins are capable of inhibiting the induction of IFN(51, 53, 55, 58-64). However, some
372 groups have observed the opposite, whereby MeV induces potent IFN expression(42, 54). In
373 general, this discrepancy has been attributed to the presence or absence of defective interfering
374 (DI) RNAs, produced as a byproduct of *in vitro* replication(51, 65, 66). Here, we found that MeV
375 induces a very potent interferon response at day 8 post infection in the presence of MeV V and C
376 transcripts. This suggests that DI RNAs generated by MeV replication in the culture may be
377 responsible for the IFN induction observed, and that this cannot be overcome by V and C at this
378 time point. One hypothesis would be that by the time DI RNAs accumulate, the IFN response is
379 too late to overcome the viral infection. Alternatively, MeV may subvert the induced IFN response
380 by utilizing the IFN-induced genes to promote pathogenesis. This idea has recently been
381 demonstrated for influenza virus, whereby the virus utilizes the host ISG IFIT2 to enhance the
382 translational efficiency of viral RNAs(67).

383 While we thoroughly characterized MeV infection and susceptibility within B and T cell
384 subsets, our study is limited in that we do not know the functional implications that MeV infection
385 in these cells has on immunologic amnesia and disease. Future work should assess the extent to
386 which MeV infection of GCBs impacts the capacity to form new germinal center responses, an
387 outcome that would compound the impact that MeV is known to have on memory B cells during
388 immunological amnesia. A second limitation of our study is that we only assessed the host
389 response to infection at the transcriptional level. Curiously, the induction of ISGs was potent in
390 both the infected and bystander cells. If MeV proteins are involved in antagonizing the host
391 response at the protein level, MeV-infected cells may differ from bystander cells at a point

392 downstream of transcription and understanding this difference may clue towards novel therapeutic
393 targets. A third limitation in our analysis is that we are unable to discern whether the differences
394 we observed in MeV infection within specific cell types could be due to cell killing by MeV rather
395 than heightened cellular susceptibility to infection. While our data suggest that susceptibility of
396 cells is positively associated with the expression of the entry receptor CD150, this does not
397 exclude the possibility that some cell types have a greater capacity to survive while infected with
398 MeV. Indeed, it has previously been established that MeV is capable of depleting CD150+ cells
399 in tonsil explants (40). Understanding this may be critical in further defining the immunological
400 correlates of pathogenesis.

401 In sum, we present a thorough elucidation of the process of MeV infection in human lymph
402 nodes, advancing our understanding of cellular susceptibility to infection. Our findings in this
403 model establish tonsil explants as a unique platform for the identification of host factors important
404 for MeV replication, and for the screening of targeted antivirals. Future work in this model should
405 focus on understanding how MeV replicates in the face of this potently induced interferon
406 response, with the goal of identifying points at which viral replication can be inhibited.

407

408 **MATERIALS AND METHODS:**

409 **Cells and plasmids:**

410 Vero-hCD150 cells were provided by Dr. Yanagi(23) at Kyushu University and maintained in
411 DMEM with 10% FBS. The genome coding plasmid for MeV (p(+) MV323-AcGFP) was kindly
412 gifted from Dr. Makoto Takeda(68). The MeV genome sequence was transferred into a pEMC
413 vector, adding an optimal T7 promotor, a hammerhead ribozyme, and an eGFP transcriptional
414 unit at the 3' end of the genome (pEMC-IC323-eGFP) as previously described(44).

415

416

417 **MeV rescue and amplification:**

418 MeV (IC323-eGFP) rescue was performed in BSR-T7 cells, seeded in 6-well format. Upon
419 confluency, pEMC-IC323eGFP (5µg), T7-MeV-N (1.2 µg), T7-MeV-P (1.2 µg), T7-MeV-L (0.4 µg),
420 a plasmid encoding a codon-optimized T7 polymerase (3 µg), PLUS reagent (5.8 µL), and
421 Lipofectamine LTX (9.3 µL) were combined in Opti-MEM (200µl; Invitrogen). After a 30min
422 incubation at RT, transfection mixture was added dropwise onto cells and incubated for 24hr at
423 37°C. Following, rescued virus was amplified once on Vero-hCD150 cells for 72hr to generate a
424 P1 virus, in infection media (made in DMEM+2% FBS). This virus was then titered (see plaque
425 assay method below) and used at an MOI = 0.01 on Vero-hCD150 cells to generate a P2 virus
426 (amplified as above). Supernatants were collected, clarified of cell debris, ultracentrifuged through
427 a 20% sucrose gradient at 24,000 RPM for 3hrs, reconstituted in fresh infection media, and frozen
428 at -80°C.

429

430 **MeV quantification by plaque assay:**

431 Vero-hCD150 were plated in 12 well format until ~90-95% confluence. 10-fold serial dilutions of
432 samples (made in DMEM+2% FBS) were applied to these monolayers in a total volume of 250µL,
433 and infections were allowed to incubate for 2hrs at 37°C. Viral inoculum was removed and
434 replaced with 500µL/well of methylcellulose (in DMEM+ 2% FBS + 7.5% $NaHCO_3$). Infections
435 proceeded for 72hrs, at which point wells were imaged for GFP^+ plaques on the Celigo S platform.

436

437 **Processing and infection of human lymphoid tissue:**

438 Human tonsils from routine tonsillectomies performed at the Mount Sinai Hospital and the New
439 York Eye and Ear Infirmary of Mount Sinai were collected under IRB-approved protocols within a
440 few hours after surgery. Tonsils were dissected into 2mm blocks, and 9 tissue blocks per well

441 were placed on top of collagen sponge gels floating in six-well plates as previously described, in
442 triplicate wells per condition(43). All 27 tissue blocks from each donor were then individually
443 inoculated with 5μl containing 1,666 PFU MeV-GFP (for a final concentration of 5,000 PFU/ml) or
444 left uninfected. Media was collected and replaced at days 3, 6 and 8 post infection for culture
445 maintenance. Tonsil donors consisted of three male and eight female donors. The median age of
446 donors was 23 years old, with a range of 4 to 54 years old. The reasons for tonsillectomy included
447 sleep apnea, breathing disorders and chronic tonsillitis.
448
449 **Visualization of MeV-infected cells in tonsillar explants by *in situ* hybridization:**
450 Tonsil blocks were collected at each time point, fixed in 10% neutral buffered formalin for 24 hrs,
451 and then replaced with PBS until paraffin embedding. *In situ* hybridization using RNAscope® was
452 performed on 5μm paraffin-embedded sections for the detection of GFP RNA. Deparaffinization
453 was performed by baking slides at 55°C for 20min. Following this step, slides were washed twice
454 with xylene for 5min each, twice in 100% ethanol for 2min each, and lastly slides were dried for
455 5min at 60°C. Slides were then incubated with hydrogen peroxide for 10min at RT and were
456 subsequently washed in diH2O. Target retrieval was performed by incubating slides in Target
457 Retrieval solution at 100°C for 15min. Slides were washed with water and transferred into 100%
458 ethanol for 3min, then were allowed to dry. Sections were treated with RNAscope® Protease Plus
459 and incubated at 40°C for 3min. Slides were then washed with diH2O. Fluorescence *in situ*
460 hybridization was subsequently performed according to the manufacturer's protocol (ACD#
461 323110) with RNAscope® Probe EGFP (ACD #400281; binds eGFP RNA) as previously
462 described (Cao et al., 2017). Following *in situ* hybridization, slides were washed twice for 5min in
463 Tris-buffered Solution containing 0.01% Tween-20 (TBST) and subsequently blocked in a solution
464 of 2.5% goat serum and 2.5% BSA in TBST for 30min at RT. Slides were then mounted with
465 Vectashield hard-set mounting medium with DAPI (Vector Laboratories) and analyzed using an
466 AxioImager Z2 microscope (Zeiss) and Zen 2012 software (Zeiss).

467 **Generating single cell suspensions from tonsil histocultures:**

468 Tonsil blocks were collected and placed in Collagenase IV, as previously described(43). Samples
469 were then placed on a thermomixer for 30min at 37°C, shaking at 500RPM. Following, samples
470 were manually homogenized with mortar and pestle prior to filtration over a 100µm cell filter. Red
471 blood cell lysis was then conducted, and cells were washed once with cold PBS. Single cell
472 suspensions were then utilized for downstream analysis.

473

474 **Single cell RNA sequencing (scRNA-Seq):**

475 Samples for scRNA-Seq were pooled for multiplex processing and analysis with a cell hashing
476 antibody strategy(69). Hash antibodies utilized were generated in house as follows: First, oligos
477 were synthesized by IDT utilizing barcode sequences from the 10x Genomics Chromium index
478 SI-GA-F11 (HBC21-29 for hash #1-8 respectively); second, oligos were coupled to antibodies
479 utilizing Thunder-Link® PLUS oligo Antibody Conjugation Kit according to manufacturer's
480 instructions. Single cell suspensions were generated from one tonsil donor at day 8 post infection
481 as described above from both infected and uninfected cultures. Dead cells were depleted from
482 samples using the EasySep™ Dead Cell Removal (Annexin V) Kit. Cells were then blocked with
483 Human TruStain FcX™ (Biolegend, 5µL/sample) as per manufacturer's protocol. Next, cells from
484 the uninfected tonsil were split into 4 hashing groups (hash #1-4), and cells from the infected
485 tonsil were split into two infected hashing groups (hash #5, 6) and two bystander hashing groups
486 (hash #7, 8). Samples were stained with corresponding hashing antibodies for 30min on ice, after
487 which unbound antibodies were removed by washing 3x in FACS buffer (PBS + 1mM EDTA + 2%
488 BSA). Cells were reconstituted in 1ml of cold FACS buffer each. Cell suspensions were filtered
489 over a 70µm filter and stained with propidium iodide (PI) for viability. Subsequently, live/GFP$^-$ cells
490 were sorted from the uninfected condition, live/GFP$^+$ cells were sorted from the infected condition,
491 and live/GFP$^-$ cells were sorted from the bystander condition. Cells were counted and 10,000 cells

492 from the uninfected condition, 5,000 cells from the infected condition, and 5,000 cells from the
493 bystander condition were pooled and processed for scRNA-Seq on the 10x Genomics Chromium
494 platform, utilizing the 10x 3' v3 kit. A scRNA-Seq library was generated as per the manufacturer's
495 protocol and sequenced on an Illumina NextSeq500 instrument. A corresponding library of
496 barcoded hash antibody oligonucleotides was indexed with a standard Ilumina D701 index and
497 sequenced as above.
498
499 **Processing of scRNA-Seq data:**
500 Raw sequencing data output (BCL files) was converted to fastq files with CellRanger mkfastq
501 v3.0.2 (10X Genomics). Per cell gene count and hashtag antibody count matrices were generated
502 with CellRanger count v3.0.2 (10X Genomics), using a human genome reference (GRCh38,
503 Ensembl v96 transcript annotations) appended with the MeV-eGFP reference and corresponding
504 transcript annotations (MeV-IC323-eGFP, Genbank: MW401770). Data were read into the R
505 statistical framework (v4.0.3) for additional analysis with Seurat(70, 71) (v4.0.1). Hashtag
506 antibody data were center log ratio normalized by feature, and individual samples were
507 demultiplexed with the Seurat HTODemux function with the positive.quantile parameter set to
508 0.99.
509
510 **Quality control and filtering of scRNA-Seq:**
511 Data exploration and HTODemux classifications were used to set QC thresholds on per cell
512 transcript unique molecular identifiers (UMI) counts, detected gene counts, and the percentage
513 of detected transcripts derived from mitochondrial genes. Cell barcodes with fewer than 2,500
514 transcript UMIs, fewer than 800 detected genes, and greater than 15% mitochondrial transcripts
515 were excluded from downstream analyses. Cell barcodes classified as negative or inter-sample
516 multiplets by HTODemux were also excluded. After filtering, these data included 5,737 cells in
517 the uninfected group, 2,736 cells in the infected group, and 2,944 in the bystander group.

518 **scRNA-Seq data analysis:**

519 Datasets were normalized with SCTransform(72), with the per cell mitochondrial transcript
520 percentage included as a regression variable. Data from all groups were integrated(70) in Seurat
521 using 3,000 anchor features; MeV genes were excluded from all integration and clustering steps
522 to avoid group-specific artifacts. Dimensionality reduction was performed by principal component
523 analysis on integrated data, and the first 20 components were selected for graph-based clustering
524 by smart local moving algorithm(73) at a resolution of 1.4 (determined by Clustering Tree
525 assessment(74)).

526 General cell types were annotated by SingleR(75) from human immune cell reference
527 data(76). Guided by SingleR annotations, prior knowledge of the cellular composition of tonsil
528 explants, flow cytometry, and exploratory gene expression analyses, clusters were assigned to
529 one of each major cell groups: T/NK, B, plasma, myeloid, stromal, and epithelial. Those major cell
530 groups with multiple component clusters were subset and re-analyzed (normalization, principal
531 components analysis dimensionality reduction, and clustering at ClusterTree determined optimal
532 resolution) for further assessment and high-resolution annotation. For each major cell group
533 subset analysis, “marker genes” distinguishing component clusters were identified by differential
534 expression analysis with the FindAllMarkers (on uninfected group for cell types that were
535 depleted/eliminated by MeV infection) and/or FindConservedMarkers (on all groups) functions.
536 Cluster annotations were assigned based on significant differential expression of canonical
537 marker genes accompanied by literature review. Intergroup differential gene expression analysis
538 was performed with edgeR(77, 78) (v3.32.1), including modifications of single cell scRNA-Seq
539 data(79). The edgeR linear model incorporated factors for cellular gene detection rate (to account
540 for scRNA-Seq “dropout”) and experimental group and included only those genes detected in at
541 least 20% of cells in any contrast condition. Statistical thresholds for significant differential gene
542 expression were set at Benjamini-Hochberg adjusted *p*-value less than 0.0001 and absolute $\log_2$
543 fold-change greater than 1.58.

544 **Immunophenotyping by flow cytometry:**

545 $3x10^6$ cells from each tonsil donor (n=3) at each time point were stained with the Zombie Red
546 fixable viability kit (Biolegend) for 10 min at RT, as per the manufacturer's protocol. Following, the
547 viability stain was washed off with cold FACS buffer, and Fc receptors were blocked with Human
548 TruStain FcX™. Samples were then split in two and stained with a B or T cell panel for 30min on
549 ice with a cocktail of antibodies against: **(B)** CD150 (Clone: A127d4; PE), CD38 (Clone: HB7; PE-
550 Cy7), CD27 (Clone: O323; APC), CD45 (Clone: HI30; BV605), CD19 (Clone: HIB19; BV750) and
551 CD3 (Clone: OKT3; BV785); **(T)** CD4 (Clone: OKT4; PerCP-Cy5.5), CD150 (Clone: A127d4; PE),
552 CXCR3 (Clone: G025H7; APC), CD45RA (Clone: HI100; AlexaFluor-700), CCR6 (Clone:
553 G034E3; APC-Cy7), CXCR5 (Clone: J252D4; BV421), CCR7 (Clone: G043H7; BV510), CD8
554 (Clone: RPA-T8; BV570), CD45 (Clone: HI30; BV605), CD19 (Clone: HIB19; BV750) and CD3
555 (Clone: OKT3; BV785). The antibody cocktail was supplemented with 1µL/reaction of Brilliant
556 Stain buffer (BD Horizon™), as per manufacturer's recommendation for bright violet fluorophores.
557 All antibodies were used at a concentration of 1µg/ml, except for CD27 (4µg/ml). Finally, cells
558 were washed 3 more times with FACS buffer, prior to fixation with BD Cytofix™ (BD Biosciences).
559 Single color controls were generated on UltraComp eBeads™ (Invitrogen™), except for GFP and
560 Live/Dead controls, which were made on cells from the infected and uninfected conditions,
561 respectively. All samples were analyzed on an Aurora Cytek®, and unmixed, compensated
562 samples were analyzed in FlowJo v10.8.1. Among $CD45^+$ cells, B and T cell subsets were defined.
563 B cell subsets identified are as follows: Naive, Germinal Center, Memory, and Activated Memory.
564 Among all T cells ($CD3^+$), $CD4^+$ helper cells, $CXCR5^+$ (pre-T_{FH} and T_{FH}), Naive $CD4^+$, T_{EMRA}, T_{EM},
565 T_{CM}, T_H1, T_H2, T_H1* and T_H17 cells were identified. In addition, $CD8^+$ cytotoxic cells, Naive $CD8^+$,
566 T_{EMRA}, T_{EM}, T_{CM} cells were identified. Full marker definitions for each B and T cell subset were
567 based upon previously published panels and are included below(36, 80):
568

569 B cells ($CD19^+$): naive ($CD27^-CD38^-$), germinal center (GCB; $CD27^-CD38^+$), memory (MBC;
570 $CD27^+CD38^-$), activated memory (AMBC; $CD27^+CD38^+$).
571
572 Helper T cells ($CD3^+CD4^+$): $CXCR5^+$ (pre-T_{FH} and T_{FH}), $CXCR5^-$, naive ($CXCR5^-$
573 $CD45RA^+CCR7^+$), effector memory RA^+ (T_{EMRA}; $CXCR5^-CD45RA^+CCR7^-$), effector memory (T_{EM};
574 $CXCR5^-CD45RA^-CCR7^-$), central memory (T_{CM}; $CXCR5^-CD45RA^-CCR7^+$), T_H1 ($CD45RA^-CCR7^-$
575 $CCR6^-CXCR3^+$), T_H1* ($CD45RA^-CCR7^-CCR6^+CXCR3^+$), T_H17 ($CD45RA^-CCR7^-CCR6^+CXCR3^-$),
576 and T_H2 ($CD45RA^-CCR7^-CCR6^-CXCR3^-$).
577

578 Cytotoxic T cells ($CD3^+CD8^+$): naive ($CD45RA^+CCR7^+$), effector memory RA^+ (T_{EMRA};
579 $CD45RA^+CCR7^-$), effector memory (T_{EM}; $CD45RA^-CCR7^-$), central memory (T_{CM}; $CD45RA^-$
580 $CCR7^+$).

581 **qRT-PCR:**

582 Total RNA was collected for two tonsil donors by resuspending single cell suspensions in 1ml of
583 TriZol. RNA was extracted and purified with the Direct-zol RNA MiniPrep Plus kit (Zymo), and 1µg
584 of RNA was reverse transcribed with random hexamer primers (Applied Biosystems). 1µl of cDNA
585 was utilized per reaction, and primer/probes for IFIT1 (HS03027069_S1), IFIT3
586 (HS01922752_S1), and MX1 (Hs00895608_m) were utilized to amplify ISG transcripts. Fold
587 induction was calculated using the ΔΔCT method by normalizing expression to GAPDH
588 expression (NC_000012.11).

589 **Statistics:**

590 Panel specific statistical testing details and sample sizes are reflected in the Fig legends. For
591 scRNA-Seq analysis, statistical analysis methodology is detailed in the above methods section.

592 For all comparison of infection susceptibility over time, significance was determined by two-way
593 ANOVA with Sidak's multiple comparison test. For all comparisons of CD150 expression among
594 multiple (>2) groups, significance was determined by one-way ANOVA with Dunnet's multiple
595 comparison test. For pair-wise comparisons, a 2-tailed paired T-test was utilized. For all statistical
596 analyses, * indicates $p<0.05$, ** indicates $p<0.01$, *** indicates $p<0.001$ and **** indicates
597 $p<0.0001$
598
599 **Study Approval:**
600 All tonsil tissues were obtained with informed consent under IRB# 16-01425-CR002 at New
601 York Eye and Ear Infirmary of Mount Sinai, or the Mount Sinai Hospital under IRB HS#12-0045.
602
603 **AUTHOR CONTRIBUTIONS:** JAA, BRR, BL and JKL conceptualized the project. JA, ARP, SH,
604 APK, PT, SI, JC, HU, BT, JRJ, BRR, BL and JKL contributed to the work intellectually. JAA, ARP,
605 SH, ASM, PT and NI conducted the experiments. SI generated the virus used in this study. BT
606 conducted tonsillectomies included in this work. JAA, ARP, SH, EJD, and BRR conducted data
607 analysis. JAA, ARP and JKL prepared the manuscript. All authors edited the manuscript.
608
609 **ACKNOWLEDGEMENTS:**
610 Research reported in this work was supported by National Institute of Allergy and Infectious
611 Disease under Award Number R01AI150837 (JKL), R21AI149033 (JKL, BRR and BL), and
612 CDMRP PR192188 (JKL and BL), and R01AI071002 (BL). JAA was supported in part by the
613 National Heart, Lung, And Blood Institute of the National Institutes of Health under Award Number
614 F31HL149295. ARP and EJD were supported in part by the National Institute of Allergy and
615 Infectious Disease under Award Number T32AI007647-23. The authors would also like to thank
616 Dr. Rachel Brody and colleagues at the Biorepository and Pathology CoRE at the Icahn School
617 of Medicine at Mount Sinai for human tissue sample collection, as well as the Human Immune

618 Monitoring Core (HIMC) at the Icahn School of Medicine at Mount Sinai for contributions to the
619 scRNA-Seq.
620

621 **REFERENCES**

622 1. Olsen LF, Truty GL, Schaffer WM. Oscillations and chaos in epidemics: A nonlinear dynamic study
623 of six childhood diseases in Copenhagen, Denmark. Theoretical Population Biology. 1988;33(3):344-70.
624 2. Merler S, Ajelli M. Deciphering the relative weights of demographic transition and vaccination in
625 the decrease of measles incidence in Italy. Proc Biol Sci. 2014;281(1777):20132676.
626 3. Edmunds WJ, Gay NJ, Kretzschmar M, Pebody RG, Wachmann H. The pre-vaccination
627 epidemiology of measles, mumps and rubella in Europe: implications for modelling studies. Epidemiol
628 Infect. 2000;125(3):635-50.
629 4. Metcalf CJ, Bjørnstad ON, Grenfell BT, Andreasen V. Seasonality and comparative dynamics of six
630 childhood infections in pre-vaccination Copenhagen. Proc Biol Sci. 2009;276(1676):4111-8.
631 5. Wallinga J, LÉVy-Bruhl D, Gay NJ, Wachmann CH. Estimation of measles reproduction ratios and
632 prospects for elimination of measles by vaccination in some Western European countries. Epidemiology
633 and Infection. 2001;127(2):281-95.
634 6. Mossong J, Muller CP. Estimation of the basic reproduction number of measles during an outbreak
635 in a partially vaccinated population. Epidemiol Infect. 2000;124(2):273-8.
636 7. Guerra FM, Bolotin S, Lim G, Heffernan J, Deeks SL, Li Y, et al. The basic reproduction number
637 (R(0)) of measles: a systematic review. Lancet Infect Dis. 2017;17(12):e420-e8.
638 8. Chovatiya R, Silverberg JI. Inpatient morbidity and mortality of measles in the United States. PLoS
639 One. 2020;15(4):e0231329-e.
640 9. Tanne JH. Measles cases and deaths are increasing worldwide, warn health agencies. Bmj.
641 2020;371:m4450.
642 10. López-Perea N, Fernández-García A, Echevarría JE, de Ory F, Pérez-Olmeda M, Masa-Calles J.
643 Measles in Vaccinated People: Epidemiology and Challenges in Surveillance and Diagnosis in the Post-
644 Elimination Phase. Spain, 2014-2020. Viruses. 2021;13(10).
645 11. Hussain A, Ali S, Ahmed M, Hussain S. The Anti-vaccination Movement: A Regression in Modern
646 Medicine. Cureus. 2018;10(7):e2919-e.
647 12. Gallegos M, de Castro Pecanha V, Caycho-Rodríguez T. Anti-vax: the history of a scientific problem.
648 J Public Health (Oxf). 2022.
649 13. Kuylen E, Willem L, Broeckhove J, Beutels P, Hens N. Clustering of susceptible individuals within
650 households can drive measles outbreaks: an individual-based model exploration. Sci Rep.
651 2020;10(1):19645.
652 14. Zucker JR, Rosen JB, Iwamoto M, Arciuolo RJ, Langdon-Embry M, Vora NM, et al. Consequences
653 of Undervaccination - Measles Outbreak, New York City, 2018-2019. N Engl J Med. 2020;382(11):1009-17.
654 15. Gaythorpe KA, Abbas K, Huber J, Karachaliou A, Thakkar N, Woodruff K, et al. Impact of COVID-
655 19-related disruptions to measles, meningococcal A, and yellow fever vaccination in 10 countries. Elife.
656 2021;10.
657 16. Rota PA, Moss WJ, Takeda M, de Swart RL, Thompson KM, Goodson JL. Measles. Nature Reviews
658 Disease Primers. 2016;2(1):16049.
659 17. Plemper RK, Snyder JP. Measles control--can measles virus inhibitors make a difference? Curr Opin
660 Investig Drugs. 2009;10(8):811-20.
661 18. Lemon K, de Vries RD, Mesman AW, McQuaid S, van Amerongen G, Yüksel S, et al. Early target
662 cells of measles virus after aerosol infection of non-human primates. PLoS Pathog. 2011;7(1):e1001263.
663 19. Ludlow M, Lemon K, de Vries RD, McQuaid S, Millar EL, van Amerongen G, et al. Measles virus
664 infection of epithelial cells in the macaque upper respiratory tract is mediated by subepithelial immune
665 cells. J Virol. 2013;87(7):4033-42.

666 20. Welstead GG, Iorio C, Draker R, Bayani J, Squire J, Vongpunsawad S, et al. Measles virus replication
667 in lymphatic cells and organs of CD150 (SLAM) transgenic mice. Proceedings of the National Academy of
668 Sciences. 2005;102(45):16415-20.
669 21. Yanagi Y, Takeda M, Ohno S, Hashiguchi T. Measles Virus Receptors. In: Griffin DE, Oldstone MBA,
670 editors. Measles: History and Basic Biology. Berlin, Heidelberg: Springer Berlin Heidelberg; 2009. p. 13-30.
671 22. Dhiman N, Jacobson RM, Poland GA. Measles virus receptors: SLAM and CD46. Rev Med Virol.
672 2004;14(4):217-29.
673 23. Ono N, Tatsuo H, Hidaka Y, Aoki T, Minagawa H, Yanagi Y. Measles Viruses on Throat Swabs from
674 Measles Patients Use Signaling Lymphocytic Activation Molecule (CDw150) but Not CD46 as a Cellular
675 Receptor. Journal of Virology. 2001;75(9):4399-401.
676 24. Takeda M, Tahara M, Nagata N, Seki F. Wild-Type Measles Virus is Intrinsically Dual-Tropic.
677 Frontiers in Microbiology. 2012;2.
678 25. Ashbaugh HR, Cherry JD, Hoff NA, Doshi RH, Alfonso VH, Gadoth A, et al. Association of Previous
679 Measles Infection With Markers of Acute Infectious Disease Among 9- to 59-Month-Old Children in the
680 Democratic Republic of the Congo. J Pediatric Infect Dis Soc. 2019;8(6):531-8.
681 26. Le NTH, Ho NT, Grenfell B, Baker S, Geskus RB. Biphasic pattern in the effect of severe measles
682 infection; the difference between additive and multiplicative scale. BMC Infect Dis. 2021;21(1):1249.
683 27. Sato R, Haraguchi M. Effect of measles prevalence and vaccination coverage on other disease
684 burden: evidence of measles immune amnesia in 46 African countries. Hum Vaccin Immunother.
685 2021;17(12):5361-6.
686 28. Morales GB, Muñoz MA. Immune amnesia induced by measles and its effects on concurrent
687 epidemics. J R Soc Interface. 2021;18(179):20210153.
688 29. de Swart RL. [The measles paradox explained: how measles virus both suppresses and activates
689 the immune system]. Ned Tijdschr Geneeskd. 2020;164.
690 30. Galassi FM, Varotto E, Mussini C, Cossarizza A. Measles-induced immune amnesia likely recorded
691 in the 18th century. J Clin Virol. 2021;141:104899.
692 31. Laksono BM, de Vries RD, Verburgh RJ, Visser EG, de Jong A, Fraaij PLA, et al. Studies into the
693 mechanism of measles-associated immune suppression during a measles outbreak in the Netherlands.
694 Nat Commun. 2018;9(1):4944.
695 32. Mina MJ, Metcalf CJ, de Swart RL, Osterhaus AD, Grenfell BT. Long-term measles-induced
696 immunomodulation increases overall childhood infectious disease mortality. Science.
697 2015;348(6235):694-9.
698 33. Mina MJ, Kula T, Leng Y, Li M, de Vries RD, Knip M, et al. Measles virus infection diminishes
699 preexisting antibodies that offer protection from other pathogens. Science. 2019;366(6465):599-606.
700 34. Von Pirquet C. FREQUENCY OF TUBERCULOSIS IN CHILDHOOD. Journal of the American Medical
701 Association. 1909;LII(9):675-8.
702 35. Valdimarsson H, Agnarsdottir G, Lachmann PJ. Measles virus receptor on human T lymphocytes.
703 Nature. 1975;255(5509):554-6.
704 36. Laksono BM, Grosserichter-Wagener C, de Vries RD, Langeveld SAG, Brem MD, van Dongen JJM,
705 et al. In Vitro Measles Virus Infection of Human Lymphocyte Subsets Demonstrates High Susceptibility and
706 Permissiveness of both Naive and Memory B Cells. J Virol. 2018;92(8).
707 37. de Swart RL, Ludlow M, de Witte L, Yanagi Y, van Amerongen G, McQuaid S, et al. Predominant
708 infection of CD150+ lymphocytes and dendritic cells during measles virus infection of macaques. PLoS
709 Pathog. 2007;3(11):e178.
710 38. de Vries RD, McQuaid S, van Amerongen G, Yüksel S, Verburgh RJ, Osterhaus ADME, et al. Measles
711 Immune Suppression: Lessons from the Macaque Model. PLOS Pathogens. 2012;8(8):e1002885.
712 39. Victora GD, Nussenzweig MC. Germinal Centers. Annual Review of Immunology. 2022;40(1):413-
713 42.

714 40. Condack C, Grivel J-C, Devaux P, Margolis L, Cattaneo R. Measles Virus Vaccine Attenuation:
715 Suboptimal Infection of Lymphatic Tissue and Tropism Alteration. The Journal of Infectious Diseases.
716 2007;196(4):541-9.
717 41. Grivel J-C, García M, Moss WJ, Margolis LB. Inhibition of HIV-1 Replication in Human Lymphoid
718 Tissues Ex Vivo by Measles Virus. The Journal of Infectious Diseases. 2005;192(1):71-8.
719 42. Hippee CE, Singh BK, Thurman AL, Cooney AL, Pezzulo AA, Cattaneo R, et al. Measles virus exits
720 human airway epithelia within dislodged metabolically active infectious centers. PLoS Pathog.
721 2021;17(8):e1009458.
722 43. Grivel J-C, Margolis L. Use of human tissue explants to study human infectious agents. Nature
723 Protocols. 2009;4(2):256-69.
724 44. Ikegame S, Hashiguchi T, Hung C-T, Dobrindt K, Brennand KJ, Takeda M, et al. Fitness selection of
725 hyperfusogenic measles virus F proteins associated with neuropathogenic phenotypes. Proceedings of the
726 National Academy of Sciences. 2021;118(18):e2026027118.
727 45. Okamoto Y, Vricella LA, Moss WJ, Griffin DE. Immature CD4+CD8+ Thymocytes Are Preferentially
728 Infected by Measles Virus in Human Thymic Organ Cultures. PLOS ONE. 2012;7(9):e45999.
729 46. Welstead GG, Hsu EC, Iorio C, Bolotin S, Richardson CD. Mechanism of CD150 (SLAM) down
730 regulation from the host cell surface by measles virus hemagglutinin protein. J Virol. 2004;78(18):9666-
731 74.
732 47. Tanaka K, Minagawa H, Xie MF, Yanagi Y. The measles virus hemagglutinin downregulates the
733 cellular receptor SLAM (CD150). Archives of Virology. 2002;147(1):195-203.
734 48. Overgaard NH, Jung J-W, Steptoe RJ, Wells JW. CD4+/CD8+ double-positive T cells: more than just
735 a developmental stage? J Leukocyte Biol. 2015;97(1):31-8.
736 49. Chevalier N, Jarrossay D, Ho E, Avery DT, Ma CS, Yu D, et al. CXCR5 Expressing Human Central
737 Memory CD4 T Cells and Their Relevance for Humoral Immune Responses. The Journal of Immunology.
738 2011;186(10):5556-68.
739 50. Griffin DE. Measles immunity and immunosuppression. Curr Opin Virol. 2021;46:9-14.
740 51. Nakatsu Y, Takeda M, Ohno S, Shirogane Y, Iwasaki M, Yanagi Y. Measles Virus Circumvents the
741 Host Interferon Response by Different Actions of the C and V Proteins. Journal of Virology.
742 2008;82(17):8296-306.
743 52. Auwaerter PG, Rota PA, Elkins WR, Adams RJ, DeLozier T, Shi Y, et al. Measles virus infection in
744 rhesus macaques: altered immune responses and comparison of the virulence of six different virus strains.
745 J Infect Dis. 1999;180(4):950-8.
746 53. Naniche D, Yeh A, Eto D, Manchester M, Friedman RM, Oldstone MB. Evasion of host defenses by
747 measles virus: wild-type measles virus infection interferes with induction of Alpha/Beta interferon
748 production. J Virol. 2000;74(16):7478-84.
749 54. Herschke F, Plumet S, Duhen T, Azocar O, Druelle J, Laine D, et al. Cell-cell fusion induced by
750 measles virus amplifies the type I interferon response. J Virol. 2007;81(23):12859-71.
751 55. Shivakoti R, Hauer D, Adams RJ, Lin W-HW, Duprex WP, de Swart RL, et al. Limited In Vivo
752 Production of Type I or Type III Interferon After Infection of Macaques with Vaccine or Wild-Type Strains
753 of Measles Virus. Journal of Interferon & Cytokine Research. 2014;35(4):292-301.
754 56. Laksono BM, de Vries RD, McQuaid S, Duprex WP, de Swart RL. Measles Virus Host Invasion and
755 Pathogenesis. Viruses. 2016;8(8).
756 57. Petrova VN, Sawatsky B, Han AX, Laksono BM, Walz L, Parker E, et al. Incomplete genetic
757 reconstitution of B cell pools contributes to prolonged immunosuppression after measles. Sci Immunol.
758 2019;4(41).
759 58. Rabaan AA, Mutair AA, Alhumaid S, Garout M, Alsubki RA, Alshahrani FS, et al. Updates on Measles
760 Incidence and Eradication: Emphasis on the Immunological Aspects of Measles Infection. Medicina
761 (Kaunas). 2022;58(5):680.

762 59. Fontana JM, Bankamp B, Bellini WJ, Rota PA. Regulation of interferon signaling by the C and V
763 proteins from attenuated and wild-type strains of measles virus. Virology. 2008;374(1):71-81.
764 60. Komune N, Ichinohe T, Ito M, Yanagi Y. Measles Virus V Protein Inhibits NLRP3 Inflammasome-
765 Mediated Interleukin-1β Secretion. Journal of Virology. 2011;85(24):13019-26.
766 61. Sparrer KM, Pfaller CK, Conzelmann KK. Measles virus C protein interferes with Beta interferon
767 transcription in the nucleus. J Virol. 2012;86(2):796-805.
768 62. Runge S, Sparrer KM, Lässig C, Hembach K, Baum A, García-Sastre A, et al. In vivo ligands of MDA5
769 and RIG-I in measles virus-infected cells. PLoS Pathog. 2014;10(4):e1004081.
770 63. Plumet S, Herschke F, Bourhis JM, Valentin H, Longhi S, Gerlier D. Cytosolic 5'-triphosphate ended
771 viral leader transcript of measles virus as activator of the RIG I-mediated interferon response. PLoS One.
772 2007;2(3):e279.
773 64. Shaffer JA, Bellini WJ, Rota PA. The C protein of measles virus inhibits the type I interferon
774 response. Virology. 2003;315(2):389-97.
775 65. Calain P, Curran J, Kolakofsky D, Roux L. Molecular cloning of natural paramyxovirus copy-back
776 defective interfering RNAs and their expression from DNA. Virology. 1992;191(1):62-71.
777 66. Pfaller CK, Mastorakos GM, Matchett WE, Ma X, Samuel CE, Cattaneo R, et al. Measles Virus
778 Defective Interfering RNAs Are Generated Frequently and Early in the Absence of C Protein and Can Be
779 Destabilized by Adenosine Deaminase Acting on RNA-1-Like Hypermutations. Journal of Virology.
780 2015;89(15):7735-47.
781 67. Tran V, Ledwith MP, Thamamongood T, Higgins CA, Tripathi S, Chang MW, et al. Influenza virus
782 repurposes the antiviral protein IFIT2 to promote translation of viral mRNAs. Nat Microbiol.
783 2020;5(12):1490-503.
784 68. Seki F, Yamada K, Nakatsu Y, Okamura K, Yanagi Y, Nakayama T, et al. The SI Strain of Measles
785 Virus Derived from a Patient with Subacute Sclerosing Panencephalitis Possesses Typical Genome
786 Alterations and Unique Amino Acid Changes That Modulate Receptor Specificity and Reduce Membrane
787 Fusion Activity. Journal of Virology. 2011;85(22):11871-82.
788 69. Stoeckius M, Zheng S, Houck-Loomis B, Hao S, Yeung BZ, Mauck WM, et al. Cell Hashing with
789 barcoded antibodies enables multiplexing and doublet detection for single cell genomics. Genome
790 Biology. 2018;19(1):224.
791 70. Stuart T, Butler A, Hoffman P, Hafemeister C, Papalexi E, Mauck WM, 3rd, et al. Comprehensive
792 Integration of Single-Cell Data. Cell. 2019;177(7):1888-902.e21.
793 71. Butler A, Hoffman P, Smibert P, Papalexi E, Satija R. Integrating single-cell transcriptomic data
794 across different conditions, technologies, and species. Nat Biotechnol. 2018;36(5):411-20.
795 72. Hafemeister C, Satija R. Normalization and variance stabilization of single-cell RNA-seq data using
796 regularized negative binomial regression. Genome Biol. 2019;20(1):296.
797 73. Waltman L, van Eck NJ. A smart local moving algorithm for large-scale modularity-based
798 community detection. The European Physical Journal B. 2013;86(11):471.
799 74. Zappia L, Oshlack A. Clustering trees: a visualization for evaluating clusterings at multiple
800 resolutions. Gigascience. 2018;7(7).
801 75. Aran D, Looney AP, Liu L, Wu E, Fong V, Hsu A, et al. Reference-based analysis of lung single-cell
802 sequencing reveals a transitional profibrotic macrophage. Nat Immunol. 2019;20(2):163-72.
803 76. Monaco G, Lee B, Xu W, Mustafah S, Hwang YY, Carré C, et al. RNA-Seq Signatures Normalized by
804 mRNA Abundance Allow Absolute Deconvolution of Human Immune Cell Types. Cell Rep.
805 2019;26(6):1627-40.e7.
806 77. McCarthy DJ, Chen Y, Smyth GK. Differential expression analysis of multifactor RNA-Seq
807 experiments with respect to biological variation. Nucleic Acids Res. 2012;40(10):4288-97.
808 78. Robinson MD, McCarthy DJ, Smyth GK. edgeR: a Bioconductor package for differential expression
809 analysis of digital gene expression data. Bioinformatics. 2009;26(1):139-40.

810 79. Soneson C, Robinson MD. Bias, robustness and scalability in single-cell differential expression
811 analysis. Nature Methods. 2018;15(4):255-61.
812 80. Wagar LE, Salahudeen A, Constantz CM, Wendel BS, Lyons MM, Mallajosyula V, et al. Modeling
813 human adaptive immune responses with tonsil organoids. Nature Medicine. 2021;27(1):125-35.

814

815

816 **FIGS**

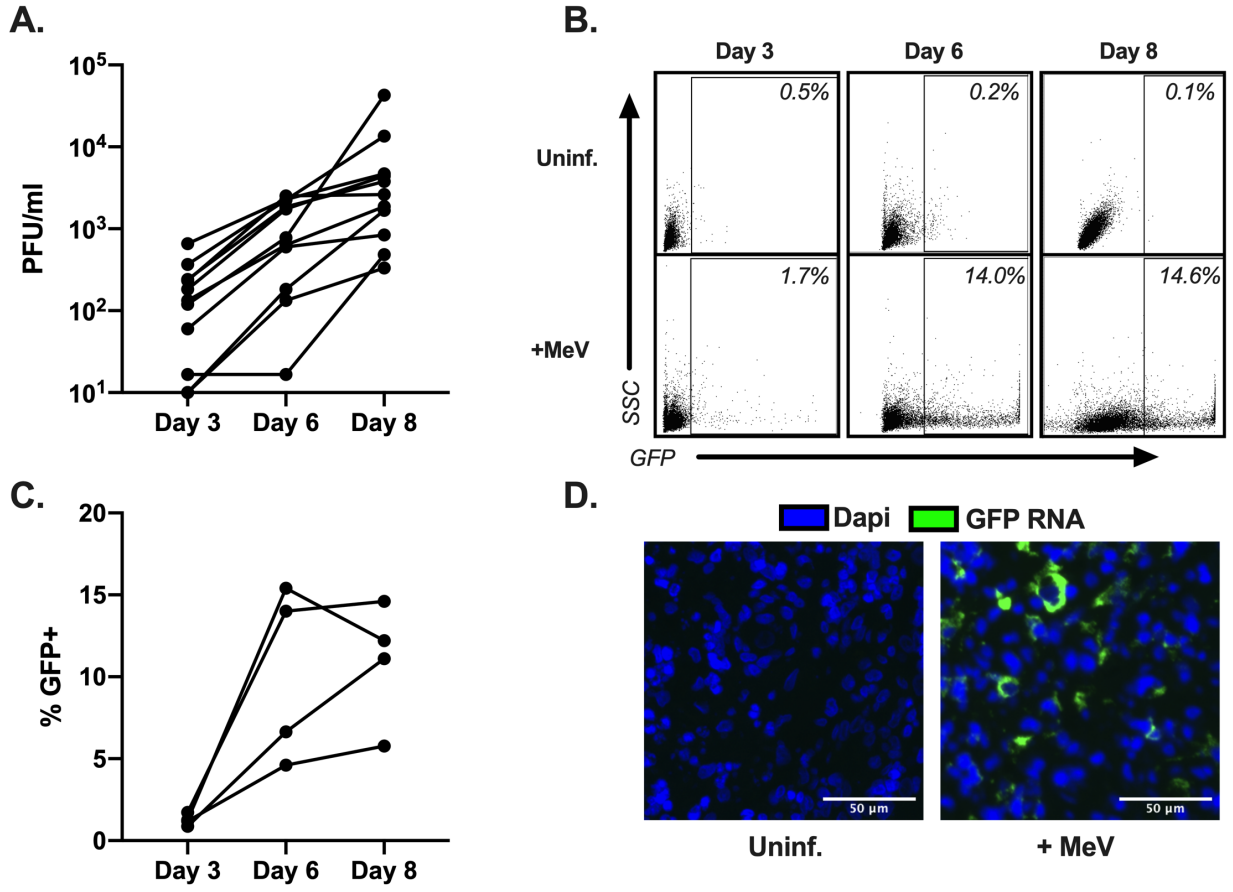

817
818 **Fig 1: MeV productively infects human lymphoid tissue explants.** Tonsil tissues from 11
819 donors were infected with MeV. Infectious virus was quantified from supernatants collected on
820 days 3, 6, and 8 post infection by plaque assay (A). Data are shown as cumulative plaque forming
821 units (PFU)/ml. Tissue explants were homogenized into single cell suspensions, and GFP^+ cells
822 were quantified by flow cytometry. Representative dot plots are shown for MeV-infected and
823 donor-matched uninfected tissue for a single donor across time (B) and quantified for a total of
824 four donors in (C). Infection was visualized by *in situ* hybridization for GFP RNA (green) on
825 paraffin-embedded tissues collected on day 8 post infection (D). Nuclei were counterstained with
826 DAPI (blue). Scale bars represent 50µm.
827
828
829
830
831
832
833
834
835
836
837

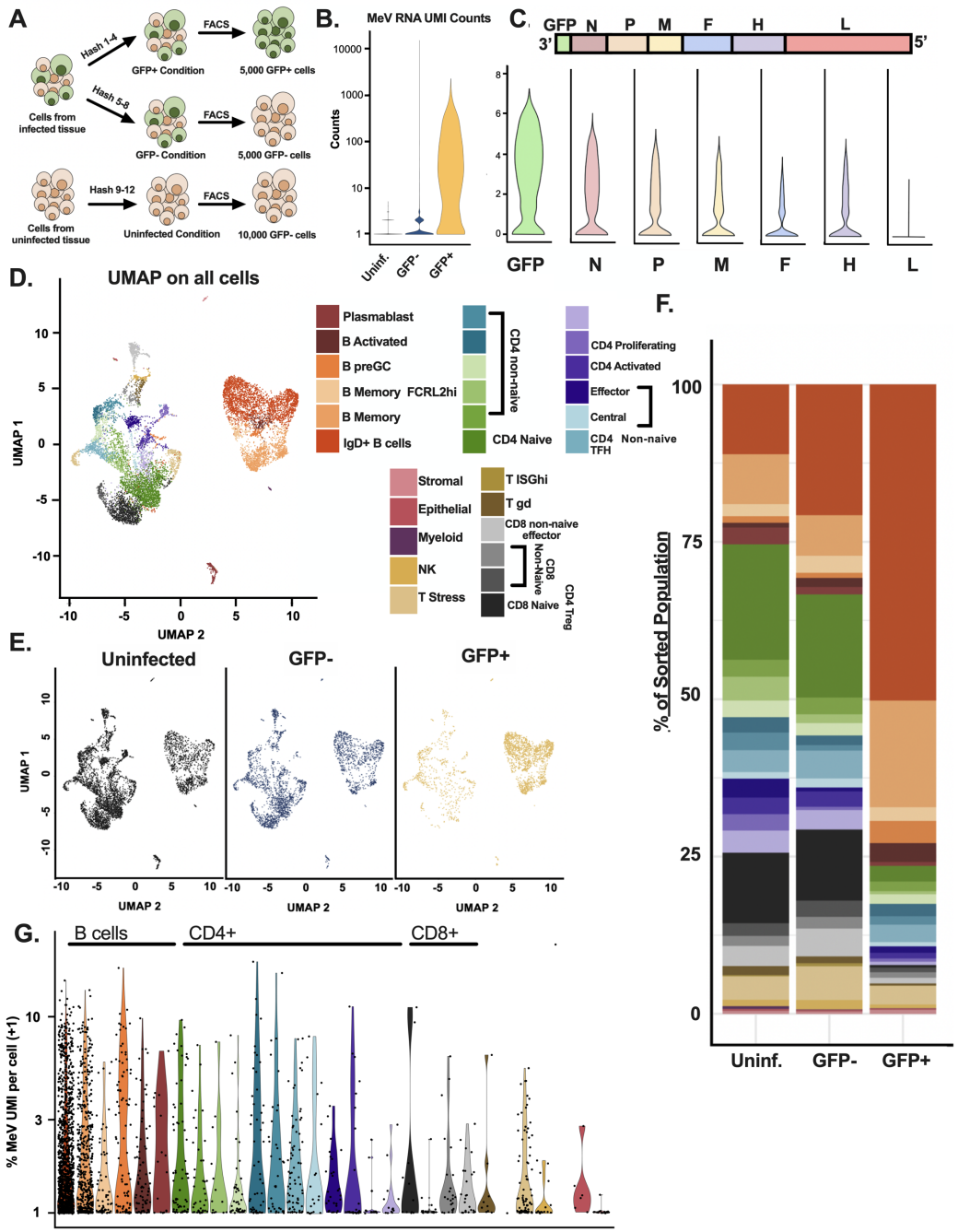

Fig 2: scRNA-Seq identifies 29 populations of tonsillar cells susceptible to MeV. Tonsil tissue from MeV-infected and uninfected explants on day 8 from one donor were prepared for scRNA-Seq. Schemata of scRNA-Seq workflow is shown in (A). MeV RNA UMIs (B) were quantified for quality control and filtering. Normalized expression of each MeV transcript in infected cells was quantified and shown as violin plots ordered from 3' to 5' in the MeV genome (C). Canonical correlation analysis (CCA) was conducted on all groups (combined) and individual clusters were functionally annotated (see also Fig S1). Clusters were visualized by UMAP (D) and then split into conditions for analysis (H). The frequencies of each cell cluster identified in (E) were calculated for each group, and quantification is shown in (F). The percentage of the transcriptome that is MeV RNA is shown in (G), with a +1 pseudocount artificially added to the values for display on a $\log_{10}$ axis.

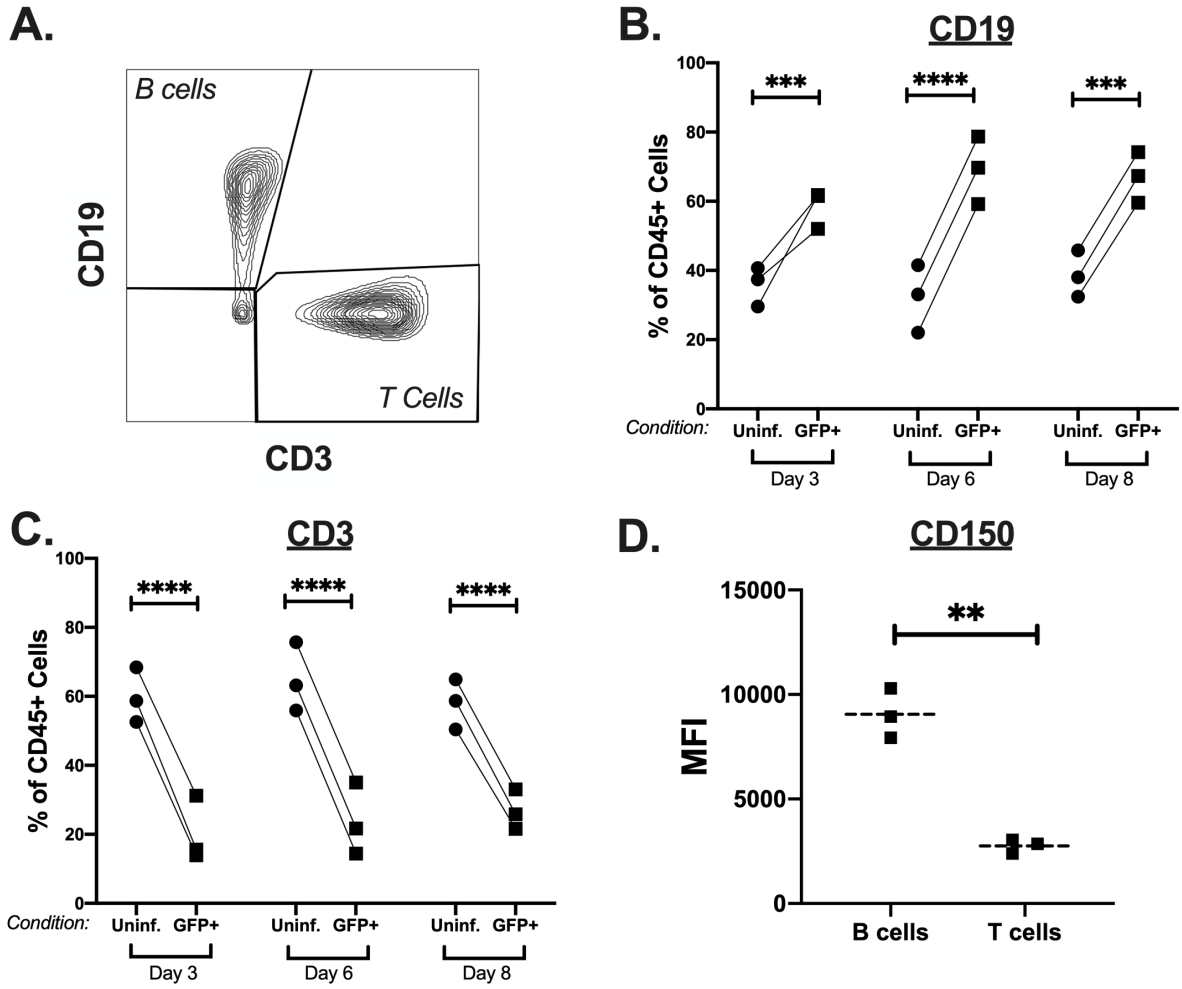

Fig 3: MeV preferentially infects CD19⁺ B cells. Single cell suspensions from MeV-infected and donor-matched uninfected tissues for 3 donors were stained with CD19 and CD3 antibodies to identify, with gating schemata is shown in (A). The frequency of $CD19^+$ cells (B) and $CD3^+$ cells (C) among both uninfected and GFP+ cells are quantified and compared over time. Significance was determined by two-way ANOVA with Sidak's multiple comparison test. The mean fluorescent intensity (MFI) of surface CD150 expression among $CD19^+$ and $CD3^+$ cells is shown (D), with significance determined by paired *t*-test. For all statistical analyses, * indicates $p<0.05$, ** indicates $p<0.01$, *** indicates $p<0.001$ and **** indicates $p<0.0001$

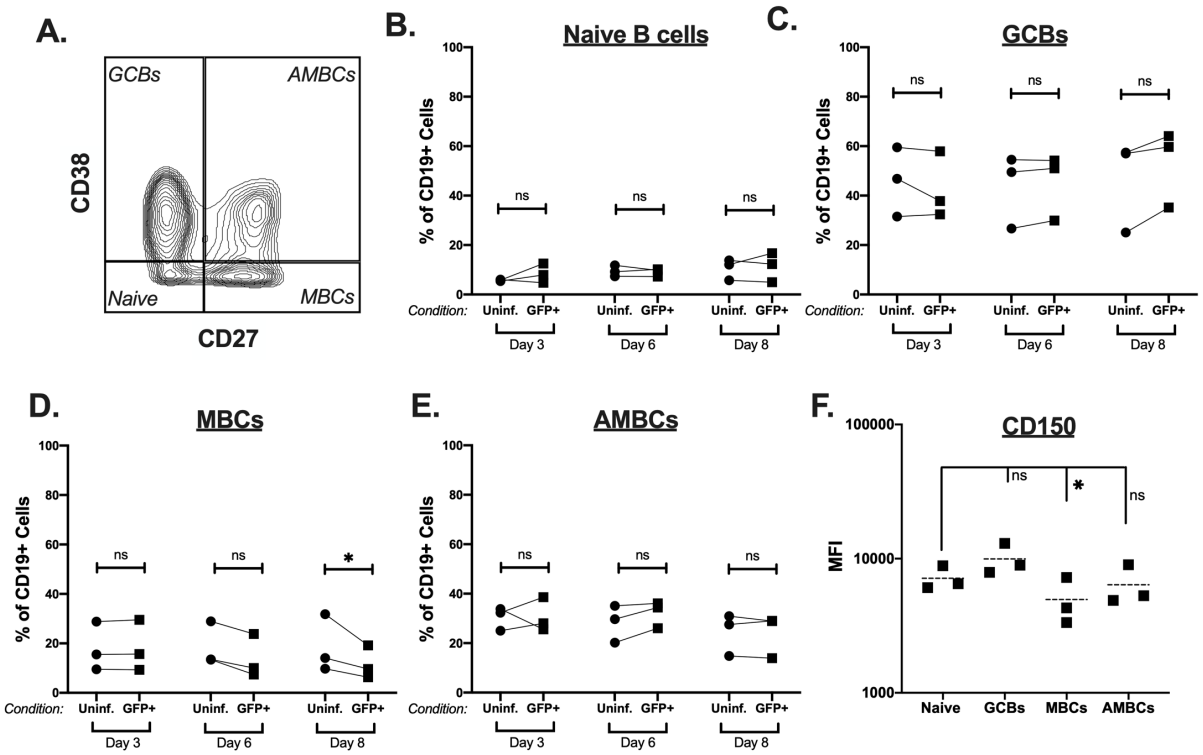

Fig 4: MeV infects B cell subsets proportionally. Single cell suspensions from MeV-infected and donor-matched uninfected tissues from 3 donors were immunophenotyped to identify B cell subsets using CD38 and CD27 within the CD19+ cells, with the gating strategy utilized is shown in (A). Naive ($CD27^{-}CD38^{-}$; B), germinal center ($CD27^{-}CD38^{-}$; C), memory ($CD27^{+}CD38^{-}$; D), and activated memory ($CD27^{+}CD38^{+}$; E) B cells were quantified by comparing the frequency of the population among both uninfected and GFP+ cells over time. Significance was determined by two-way ANOVA, with Sidak's multiple comparison test. CD150 expression was calculated for each population among uninfected cells at 6 days post infection and mean fluorescent intensity (MFI) of CD150 expression is shown (F). Significance was determined by one-way ANOVA with Dunnet's multiple comparison test. For all statistical analyses, * indicates $p<0.05$, ** indicates $p<0.01$, *** indicates $p<0.001$ and **** indicates $p<0.0001$

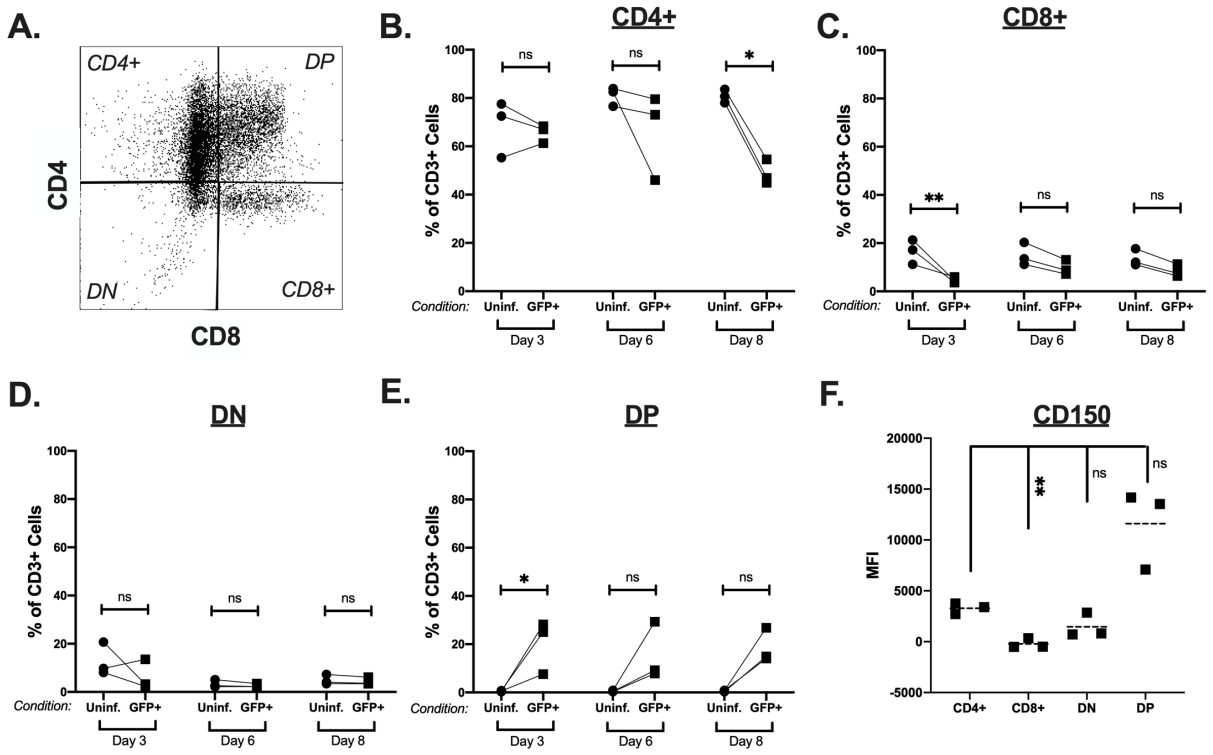

Fig 5: CD4$^+$ helper T cells are more frequently infected than CD8$^+$ cytotoxic T cells. Single cell suspensions from MeV-infected and donor-matched uninfected tissues from 3 donors were immunophenotyped to identify T cell subsets using CD4 and CD8 within the CD3+ cells, with the gating strategy utilized is shown in (A). The frequency of CD4$^+$ cells (B), CD8$^+$ cells (C) CD4/CD8 double negative cells (DN; D), and CD4/CD8 double positive (DP; E) among both uninfected and GFP+ cells are quantified and compared over time. Significance was determined by two-way ANOVA, with Sidak's multiple comparison test. The mean fluorescent intensity (MFI) of CD150 was calculated for each population among uninfected cells on day 6 and is shown (F). Significance was determined by one-way ANOVA with Dunnet's multiple comparison test. For all statistical analyses, * indicates $p<0.05$, ** indicates $p<0.01$, *** indicates $p<0.001$ and **** indicates $p<0.0001$

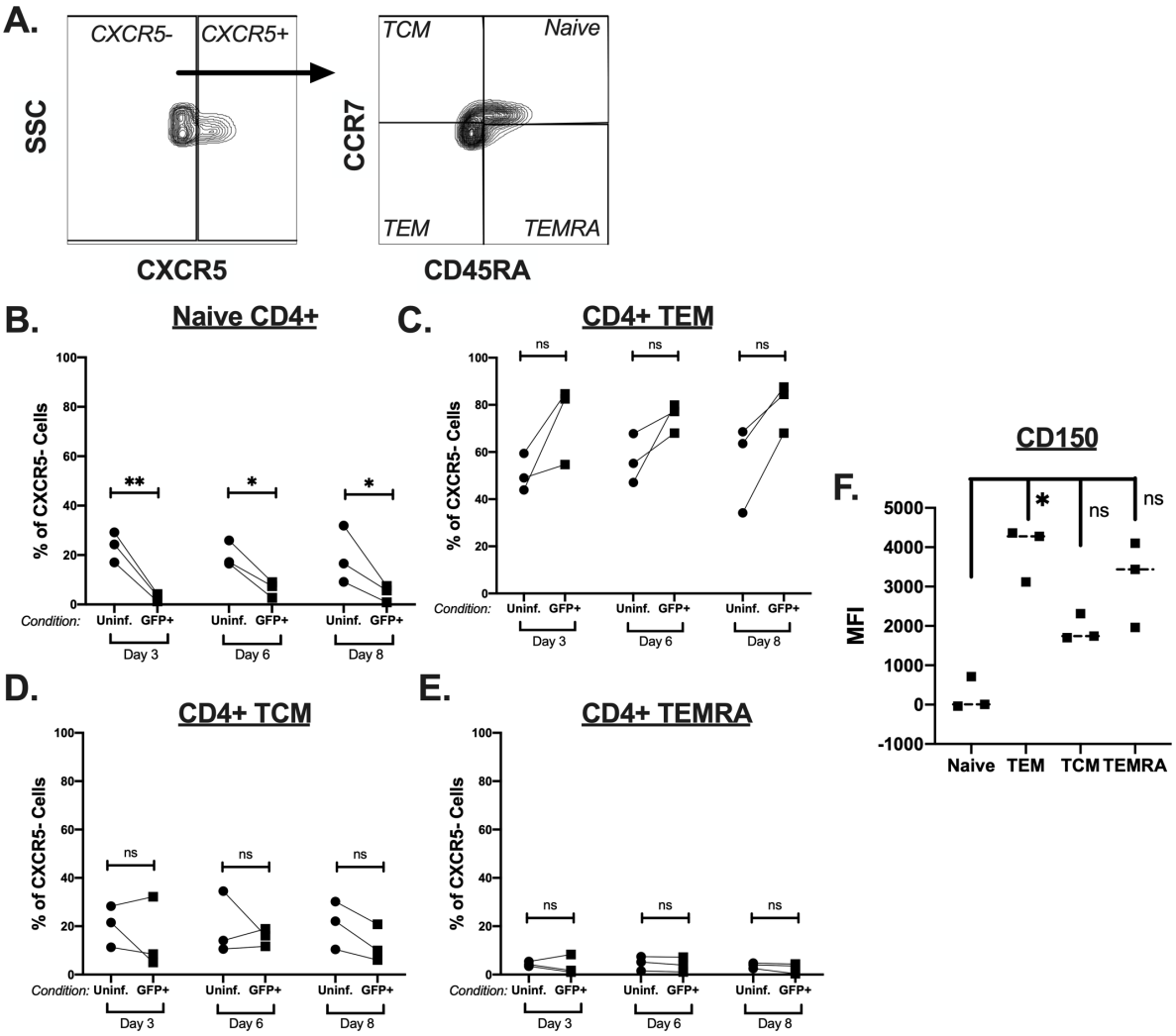

Fig 6: Naïve CD4+ Cells are less susceptible to MeV than other CD4$^+$ subsets. Single cell suspensions from MeV-infected and donor-matched uninfected tissues from 3 donors were immunophenotyped to identify T cell subsets within the CD4+ cells. CD4$^+$ cells were subset first based on CXCR5 expression, and then based expression of CD45RA and CCR7, with the gating strategy shown in (A). The frequencies of naive (B), T_{EM} (C), T_{CM} (D) and T_{EMRA} (E) cells among both uninfected and GFP+ cells are quantified and compared over time. The MFI of CD150 expression on naive and T_{EM} cells was compared (F), with significance determined by paired-t test. Significance for (B-C) was determined by two-way ANOVA, with Sidak's multiple comparison test. For all statistical analyses, * indicates $p<0.05$, ** indicates $p<0.01$, *** indicates $p<0.001$ and **** indicates $p<0.0001$.

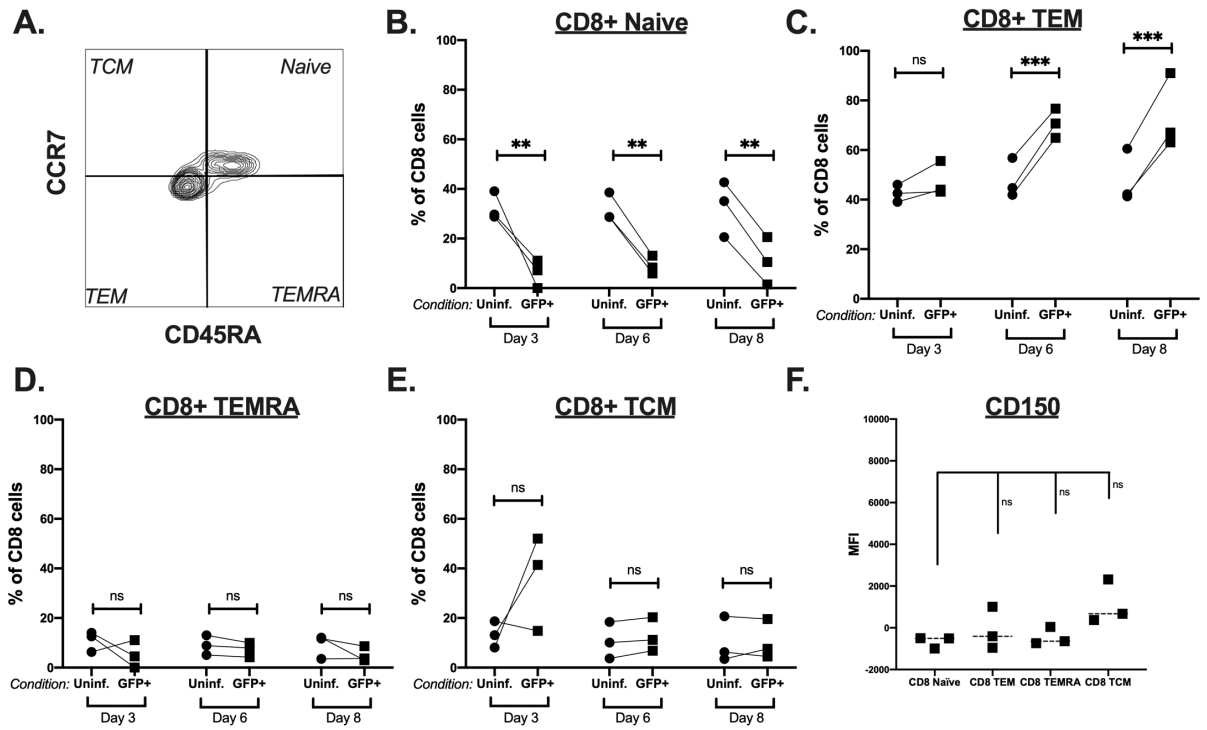

Fig 7: MeV infection among CD8+ T cell subsets is biased towards memory cells. Single cell suspensions from MeV-infected and donor-matched uninfected tissues from 3 donors were immunophenotyped to identify T cell subsets within the CD8+ cells. $CD8^+$ cells were subset based expression of CD45RA and CCR7, with the gating strategy shown in (A). The frequencies of naive (B) and T_{EM} (C), T_{EMRA} (D), and T_{CM} (E) cells among both uninfected and GFP+ cells are quantified and compared over time. The expression of CD150 was compared between each cell subset, as shown by MFI in (F). Significance for (B-E) was determined by two-way ANOVA, with Sidak's multiple comparison test. Significance for F was determined by one-way ANOVA with Dunnet's multiple comparison test. For all statistical analyses, * indicates $p<0.05$, ** indicates $p<0.01$, *** indicates $p<0.001$ and **** indicates $p<0.0001$.

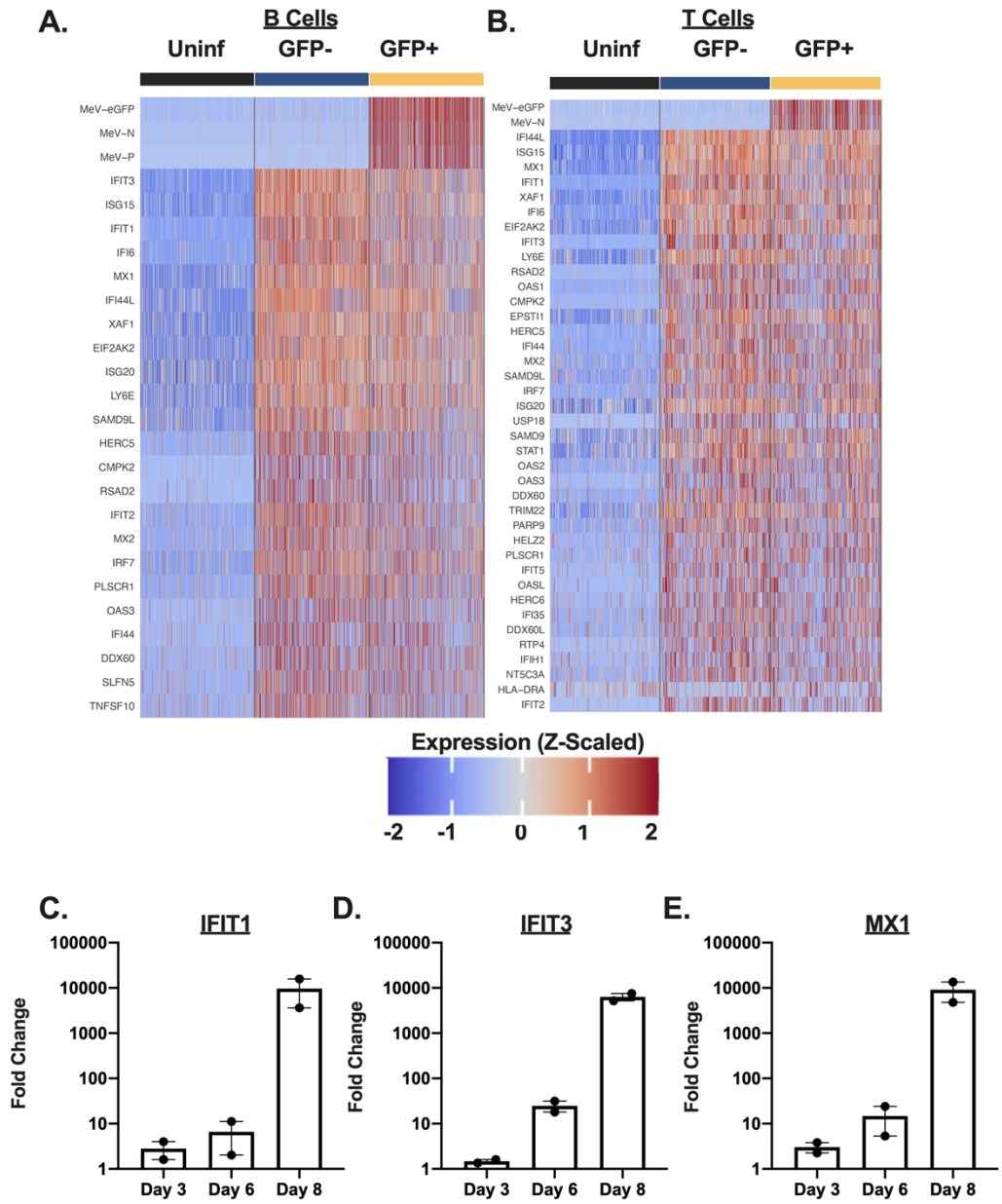

Fig 8: Host response to MeV in tonsil explants is dominated by interferon signaling. All B cell clusters from the scRNA-Seq shown in Fig 2 were combined (with stochastic downsampling), as were all T cell clusters. Differential gene expression analysis was conducted with EdgeR, and expression of the most significant genes is shown by heat map (A for B cells, B for T cells). Statistical thresholds for significant differential gene expression were set at Benjamini-Hochberg adjusted *p* value less than 0.0001 and absolute $\log_2$ fold-change greater than 1.58. Total RNA from two additional donors was collected and examined for the expression of IFIT1 (C), IFIT3 (D) and MX1 (E) by qRT-PCR at days 3, 6 and 8 post infection. The fold change in expression levels is shown, with the expression of each ISG normalized to the expression of GAPDH (ΔΔCT method).

SUPPLEMENTAL MATERIAL

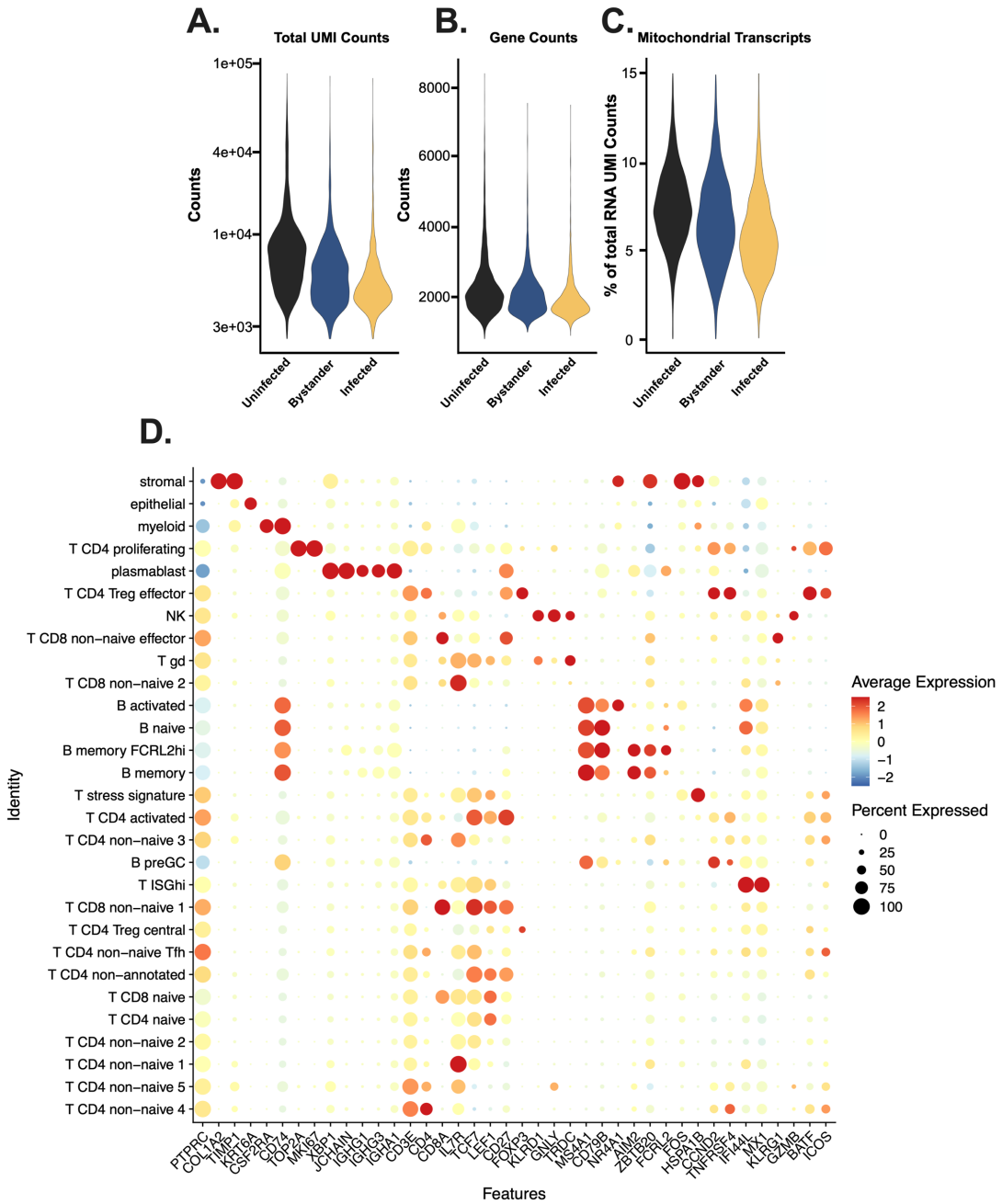

Fig S1: Cluster annotation strategy for scRNA-Seq. Total counts of unique molecular identifiers (UMI; A), individual genes (B), and mitochondrial transcripts (C) were quantified for quality control and filtering. (D) Dot plot showing the expression of cluster defining features across each identified cell cluster. Average expression (Z scaled) is shown for each feature by color, while the percentage of cells in each cluster expressing that feature is shown by the size of the dot.

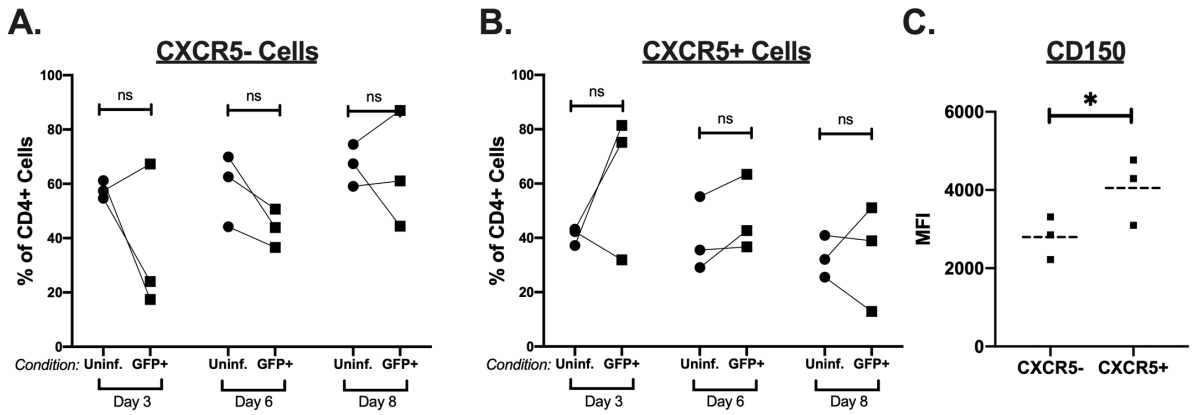

Fig S2: There are no differences in susceptibility to MeV infection based on CXCR5 expression. The frequencies of CD4+ T cells that do not express (A) or express (B) CXCR5 among uninfected (GFP^- from uninfected tonsil) or infected cells (GFP^+ in MeV-infected tonsil) were quantified and compared over time. Significance was determined by two-way ANOVA, with Sidak's multiple comparison test. In addition, these groups were compared based on their relative expression of CD150, shown by MFI (C), with significance determined by one-way ANOVA with Dunnet's multiple comparison test. For all statistical analyses, * indicates $p<0.05$, ** indicates $p<0.01$, *** indicates $p<0.001$ and **** indicates $p<0.0001$.

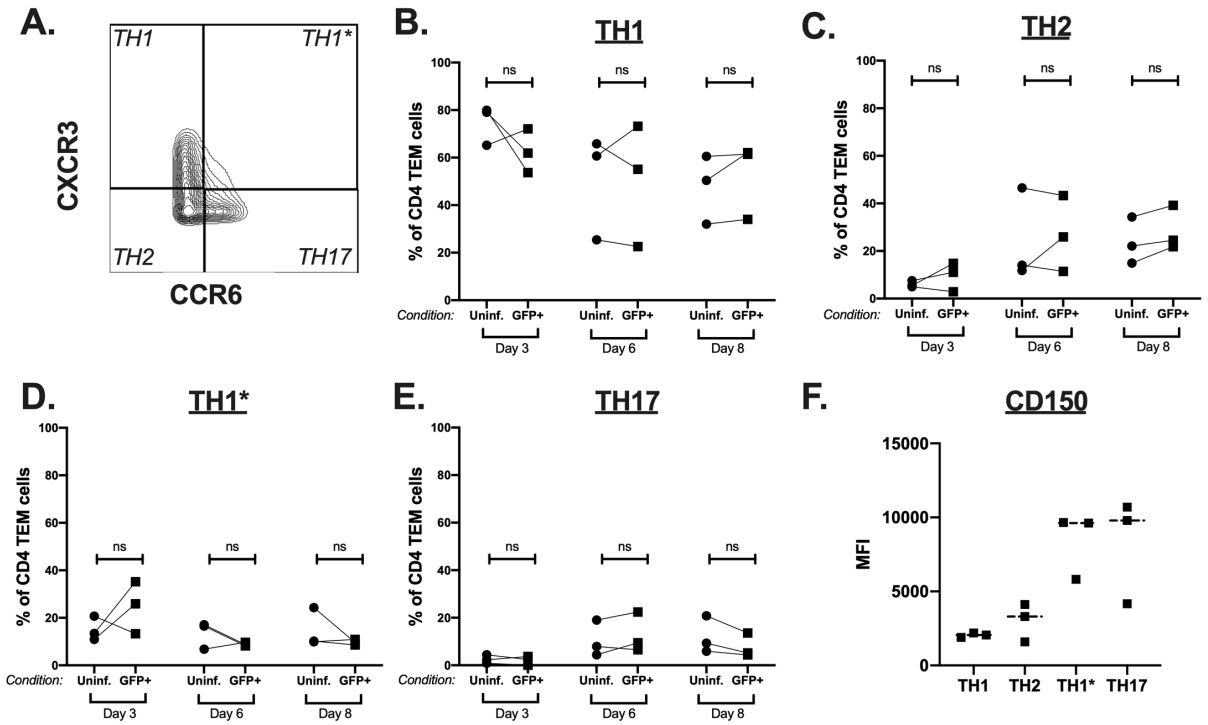

994
995 **Fig S3: There are no differenes in susceptibility to MeV infection among CD4$^+$ T$_{EM}$ subsets.**
996 CD4$^+$ T$_{EM}$ cells were further phenotyped into T$_H$1 (B), T$_H$2 (C), T$_H$1* (D), and T$_H$17 (E) cells to
997 compare their frequencies among uninfected and MeV-infected CD4$^+$ T$_{EM}$ cells. MFI of surface
998 CD150 expression shown for each subset (F), with significance determined by one-way ANOVA
999 with Dunnet's multiple comparison test. For all statistical analyses, * indicates $p<0.05$, ** indicates
1000 $p<0.01$, *** indicates $p<0.001$ and **** indicates $p<0.0001$.
1001

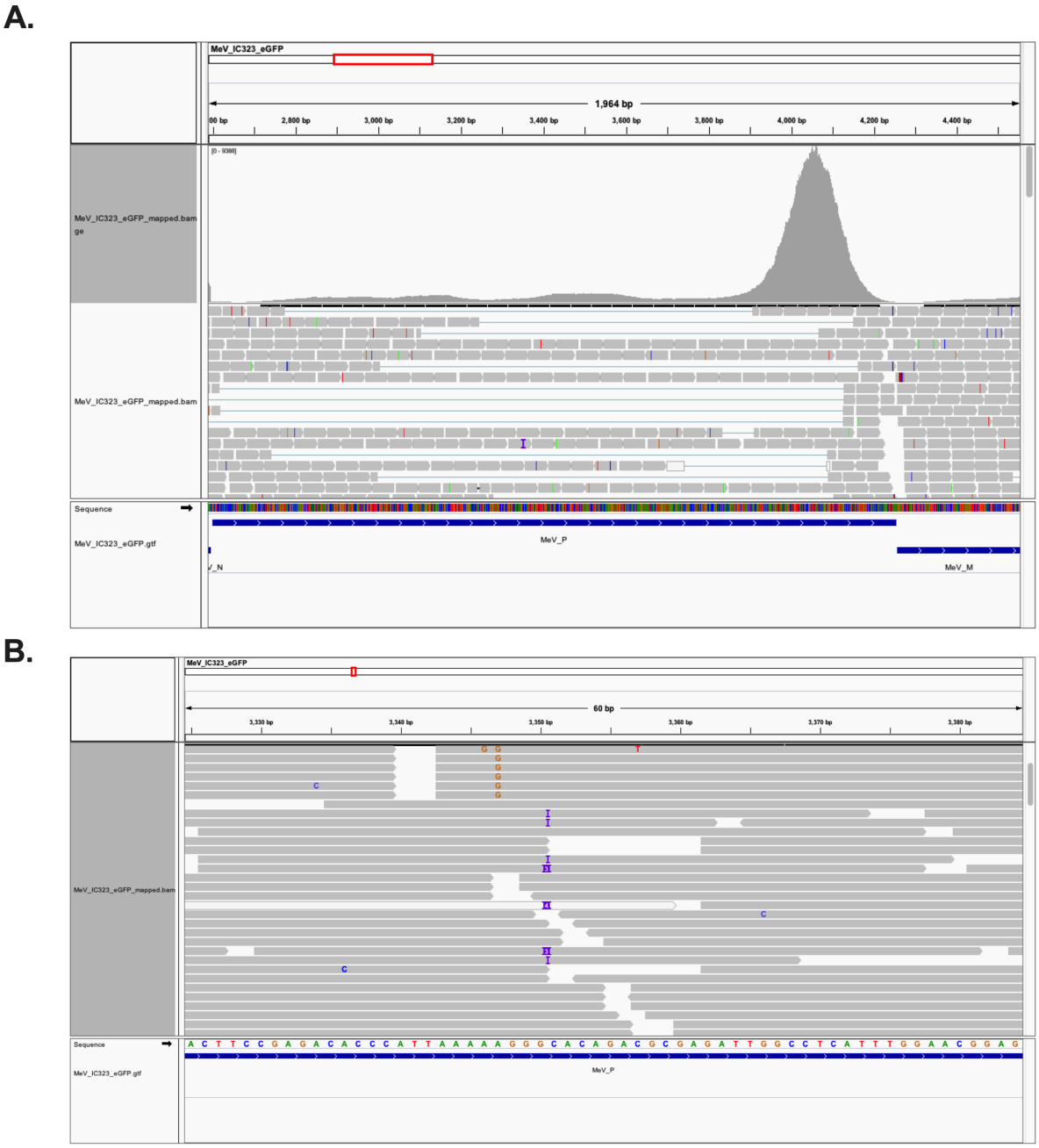

Fig S4: Detection of P-editing by scRNA-Seq. (A) Read coverage for all libraries along the entire length of the MeV P transcript. The red box denotes the region of the MeV linear genome that is shown in the histogram box, and the boxes under the histogram are a selection of reads that map to these positions. Grey bars indicate that the read matches to the reference sequence, with colored letters representing mismatches to the reference. (B) Zoomed-in coverage of the p-edited region, showing representative reads that map to this region of the gene in grey. "I" represents indel mappings, which may indicate P-edited transcripts. There were 235 total reads covering the putative edit site. Also of note, slightly upstream at MeV_IC323_eGFP:3347, the final reference A has a significant portion of reads (~9%) containing a "G" - likely also indicating editing.